ACCEPTED FOR PUBLICATION IN *The Astrophysical Journal* LBNL-41801
Preprint typeset using LaTeX style emulateapj

MEASUREMENTS OF Ω AND Λ FROM 42 HIGH-REDSHIFT SUPERNOVAE

S. PERLMUTTER[1], G. ALDERING, G. GOLDHABER[1], R.A. KNOP, P. NUGENT,
P. G. CASTRO[2], S. DEUSTUA, S. FABBRO[3], A. GOOBAR[4],
D. E. GROOM, I. M. HOOK[5], A. G. KIM[1,6], M. Y. KIM, J. C. LEE[7],
N. J. NUNES[2], R. PAIN[3], C. R. PENNYPACKER[8], R. QUIMBY
Institute for Nuclear and Particle Astrophysics,
E. O. Lawrence Berkeley National Laboratory, Berkeley, California 94720.
C. LIDMAN
European Southern Observatory, La Silla, Chile.
R. S. ELLIS, M. IRWIN, R. G. MCMAHON
Institute of Astronomy, Cambridge, United Kingdom.
P. RUIZ-LAPUENTE
Department of Astronomy, University of Barcelona, Barcelona, Spain.
N. WALTON
Isaac Newton Group, La Palma, Spain.
B. SCHAEFER
Department of Astronomy, Yale University, New Haven, Connecticut.
B. J. BOYLE
Anglo-Australian Observatory, Sydney, Australia.
A. V. FILIPPENKO, T. MATHESON
Department of Astronomy, University of California, Berkeley, CA.
A. S. FRUCHTER, N. PANAGIA[9]
Space Telescope Science Institute, Baltimore, Maryland.
H. J. M. NEWBERG
Fermi National Laboratory, Batavia, Illinois.
W. J. COUCH
University of New South Wales, Sydney, Australia.
(THE SUPERNOVA COSMOLOGY PROJECT)

Accepted for publication in The Astrophysical Journal *LBNL-41801*

ABSTRACT

We report measurements of the mass density, Ω_M, and cosmological-constant energy density, Ω_Λ, of the universe based on the analysis of 42 Type Ia supernovae discovered by the Supernova Cosmology Project. The magnitude-redshift data for these supernovae, at redshifts between 0.18 and 0.83, are fit jointly with a set of supernovae from the Calán/Tololo Supernova Survey, at redshifts below 0.1, to yield values for the cosmological parameters. All supernova peak magnitudes are standardized using a SN Ia lightcurve width-luminosity relation. The measurement yields a joint probability distribution of the cosmological parameters that is approximated by the relation $0.8\,\Omega_M - 0.6\,\Omega_\Lambda \approx -0.2 \pm 0.1$ in the region of interest ($\Omega_M \lesssim 1.5$). For a flat ($\Omega_M + \Omega_\Lambda = 1$) cosmology we find $\Omega_M^{\rm flat} = 0.28^{+0.09}_{-0.08}$ (1σ statistical) $^{+0.05}_{-0.04}$ (identified systematics). The data are strongly inconsistent with a $\Lambda = 0$ flat cosmology, the simplest inflationary universe model. An open, $\Lambda = 0$ cosmology also does not fit the data well: the data indicate that the cosmological constant is non-zero and positive, with a confidence of $P(\Lambda > 0) = 99\%$, including the identified systematic uncertainties. The best-fit age of the universe relative to the Hubble time is $t_0^{\rm flat} = 14.9^{+1.4}_{-1.1}(0.63/h)$ Gyr for a flat cosmology. The size of our sample allows us to perform a variety of statistical tests to check for possible systematic errors and biases. We find no significant differences in either the host reddening distribution or Malmquist bias between the low-redshift Calán/Tololo sample and our high-redshift sample. Excluding those few supernovae which are outliers in color excess or fit residual does not significantly change the results. The conclusions are also robust whether or not a width-luminosity relation is used to standardize the supernova peak magnitudes. We discuss, and constrain where possible, hypothetical alternatives to a cosmological constant.

[1]Center for Particle Astrophysics, U.C. Berkeley, California.
[2]Instituto Superior Técnico, Lisbon, Portugal.
[3]LPNHE, CNRS-IN2P3 & University of Paris VI & VII, Paris, France.
[4]Department of Physics, University of Stockholm, Stockholm, Sweden.
[5]European Southern Observatory, Munich, Germany.
[6]PCC, CNRS-IN2P3 & Collège de France, Paris, France.
[7]Institute of Astronomy, Cambridge, United Kingdom.
[8]Space Sciences Laboratory, U.C. Berkeley, California.
[9]Space Sciences Department, European Space Agency.

1. INTRODUCTION

Since the earliest studies of supernovae, it has been suggested that these luminous events might be used as standard candles for cosmological measurements (Baade 1938). At closer distances they could be used to measure the Hubble constant, if an absolute distance scale or magnitude scale could be established, while at higher redshifts they could determine the deceleration parameter (Tammann 1979; Colgate 1979). The Hubble constant measurement became a realistic possibility in the 1980's, when the more homogeneous subclass of Type Ia supernovae (SNe Ia) was identified (see Branch 1998). Attempts to measure the deceleration parameter, however, were stymied for lack of high-redshift supernovae. Even after an impressive multi-year effort by Nørgaard-Nielsen et al. (1989), it was only possible to follow one SN Ia, at $z = 0.31$, discovered 18 days past its peak brightness.

The Supernova Cosmology Project was started in 1988 to address this problem. The primary goal of the project is the determination of the cosmological parameters of the universe using the magnitude-redshift relation of Type Ia supernovae. In particular, Goobar & Perlmutter (1995) showed the possibility of separating the relative contributions of the mass density, Ω_M, and the cosmological constant, Λ, to changes in the expansion rate by studying supernovae at a range of redshifts. The Project developed techniques, including instrumentation, analysis, and observing strategies, that make it possible to systematically study high-redshift supernovae (Perlmutter et al. 1995a). As of March 1998, more than 75 Type Ia supernovae at redshifts $z = 0.18$–0.86 have been discovered and studied by the Supernova Cosmology Project (Perlmutter et al. 1995b, 1996, 1997a,b,c,d, 1998a).

A first presentation of analysis techniques, identification of possible sources of statistical and systematic errors, and first results based on seven of these supernovae at redshifts $z \sim 0.4$ were given in Perlmutter et al. (1997e; hereafter referred to as "P97"). These first results yielded a confidence region that was suggestive of a flat, $\Lambda = 0$ universe, but with a large range of uncertainty. Perlmutter et al. (1998b) added a $z = 0.83$ SN Ia to this sample, with observations from the Hubble Space Telescope and Keck 10-meter telescope, providing the first demonstration of the method of separating Ω_M and Λ contributions. This analysis offered preliminary evidence for a low-mass-density universe with a best-fit value of $\Omega_M = 0.2 \pm 0.4$, assuming $\Lambda = 0$. Independent work by Garnavich et al. (1998a), based on three supernovae at $z \sim 0.5$ and one at $z = 0.97$, also suggested a low mass density, with best-fit $\Omega_M = -0.1 \pm 0.5$ for $\Lambda = 0$.

Perlmutter et al. (1998c) presented a preliminary analysis of 33 additional high-redshift supernovae, which gave a confidence region indicating an accelerating universe, and barely including a low-mass $\Lambda = 0$ cosmology. Recent independent work of Riess et al. (1998), based on 10 high-redshift supernovae added to the Garnavich et al. set, reached the same conclusion. Here we report on the complete analysis of 42 supernovae from the Supernova Cosmology Project, including the reanalysis of our previously reported supernovae with improved calibration data and improved photometric and spectroscopic SN Ia templates.

2. BASIC DATA AND PROCEDURES

The new supernovae in this sample of 42 were all discovered while still brightening, using the Cerro Tololo 4-meter telescope with the 2048^2-pixel prime-focus CCD camera or the 4×2048^2-pixel Big Throughput Camera (Bernstein & Tyson 1998). The supernovae were followed with photometry over the peak of their lightcurves, and approximately two-to-three months further (∼40–60 days restframe) using the CTIO 4-m, WIYN 3.6-m, ESO 3.6-m, INT 2.5-m, and WHT 4.2-m telescopes. (SN 1997ap and other 1998 supernovae have also been followed with HST photometry.) The supernova redshifts and spectral identifications were obtained using the Keck I and II 10-m telescopes with LRIS (Oke et al. 1995) and the ESO 3.6-m telescope. The photometry coverage was most complete in Kron-Cousins *R*-band, with Kron-Cousins *I*-band photometry coverage ranging from two or three points near peak to relatively complete coverage paralleling the *R*-band observations.

Almost all of the new supernovae were observed spectroscopically. The confidence of the Type Ia classifications based on these spectra taken together with the observed lightcurves, ranged from "definite" (when Si II features were visible) to "likely" (when the features were consistent with Type Ia, and inconsistent with most other types). The lower confidence identifications were primarily due to host-galaxy contamination of the spectra. Fewer than 10% of the original sample of supernova candidates from which these SNe Ia were selected were confirmed to be non-Type Ia, i.e., being active galactic nuclei or belonging to another SN subclass; almost all of these non-SNe Ia could also have been identified by their lightcurves and/or position far from the SN Ia Hubble line. Whenever possible, the redshifts were measured from the narrow host-galaxy lines, rather than the broader supernova lines. The lightcurves and several spectra are shown in Perlmutter et al. (1997e, 1998c, 1998b); complete catalogs and detailed discussions of the photometry and spectroscopy for these supernovae will be presented in forthcoming papers.

The photometric reduction and the analyses of the lightcurves followed the procedures described in P97. The supernovae were observed with the Kron-Cousins filter that best matched the restframe *B* and *V* filters at the supernova's redshift, and any remaining mismatch of wavelength coverage was corrected by calculating the expected photometric difference—the "cross-filter *K*-correction"—using template SN Ia spectra, as in Kim, Goobar, & Perlmutter (1996). We have now recalculated these *K* corrections (see Nugent et al. 1998), using improved template spectra, based on an extensive database of low-redshift SN Ia spectra recently made available from the Calán/Tololo survey (Phillips et al. 1998). Where available, IUE and HST spectra (Cappellaro, Turatto, & Fernley 1995; Kirshner et al. 1993) were also added to the SN Ia spectra, including those published previously (1972E, 1981B, 1986G, 1990N, 1991T, 1992A, and 1994D in: Kirshner & Oke 1975; Branch et al. 1983; Phillips et al. 1987; Jeffery et al. 1992; Meikle et al. 1996; Patat et al. 1996). In Nugent et al. (1998) we show that the *K*-corrections can be calculated accurately for a given day on the supernova lightcurve, and for a given supernova lightcurve width, from the color of the supernova on that day. (Such a calculation of *K* correction based on supernova color will also automatically account for any modification of the *K* correction due to reddening of the supernova; see Nugent et al. 1998. In the case of insignificant reddening the SN Ia template color curves can be used.) We find that these calculations are robust to mis-estimations of the lightcurve width or day on the lightcurve, giving results correct to within 0.01 mag for lightcurve width errors of ±25% or lightcurve phase errors of ±5 days even at redshifts where filter matching is the worst. Given small additional uncertainties in the colors of supernovae, we take an overall systematic uncertainty of 0.02 magnitudes for the K correction.

The improved K-corrections have been recalculated for all the supernovae used in this paper, including those previously analyzed and published. Several of the low-redshift supernovae from the Calán/Tololo survey have relatively large changes (as much as 0.1 magnitudes) at times in their K-corrected lightcurves. (These and other low-redshift supernovae with new K-corrections are used by several independent groups in constructing SN Ia lightcurve templates, so the templates must be updated accordingly.) The K-corrections for several of the high-redshift supernovae analyzed in P97 have also changed by small amounts at the lightcurve peak ($\Delta K(t=0) \lesssim 0.02$ mag) and somewhat larger amounts by 20 days past peak ($\Delta K(t=20) \lesssim 0.1$ mag); this primarily affects the measurement of the restframe lightcurve width. These K-correction changes balance out among the P97 supernovae, so the final results for these supernovae do not change significantly. (As we discuss below, however, the much larger current dataset does affect the interpretation of these results.).

As in P97, the peak magnitudes have been corrected for the lightcurve width-luminosity relation of SNe Ia:

$$m_B^{\rm corr} = m_B + \Delta_{\rm corr}(s), \qquad (1)$$

where the correction term $\Delta_{\rm corr}$ is a simple monotonic function of the "stretch factor," s, that stretches or contracts the time axis of a template SN Ia lightcurve to best fit the observed lightcurve for each supernova (see Perlmutter et al. 1995a, 1997e; Kim et al. 1998; Goldhaber et al. 1998; and cf. Phillips 1993; Riess, Press, & Kirshner 1995, 1996). A similar relation corrects the V band lightcurve, with the same stretch factor in both bands. For the supernovae discussed in this paper, the template must be time-dilated by a factor $1+z$ before fitting to the observed lightcurves to account for the cosmological lengthening of the supernova timescale (Goldhaber et al. 1995; Leibundgut et al. 1996a; Riess et al. 1997a). P97 calculated $\Delta_{\rm corr}(s)$ by translating from s to Δm_{15} (both describing the timescale of the supernova event) and then using the relation between Δm_{15} and luminosity as determined by Hamuy et al. (1995). The lightcurves of the Calán/Tololo supernovae have since been published, and we have directly fit each lightcurve with the stretched template method to determine its stretch factor s. In this paper, for the light-curve width-luminosity relation, we therefore directly use the functional form

$$\Delta_{\rm corr}(s) = \alpha(s-1) \qquad (2)$$

and determine α simultaneously with our determination of the cosmological parameters. With this functional form, the supernova peak apparent magnitudes are thus all "corrected" as they would appear if the supernovae had the lightcurve width of the template, $s = 1$.

We use analysis procedures that are designed to be as similar as possible for the low- and high-redshift datasets. Occasionally, this requires not using all of the data available at low redshift, when the corresponding data are not accessible at high redshift. For example, the low-redshift supernova lightcurves can often be followed with photometry for many months with high signal-to-noise ratios, whereas the high-redshift supernova observations are generally only practical for approximately 60 restframe days past maximum light. This period is also the phase of the low-redshift SN Ia lightcurves that is fit best by the stretched-template method, and best predicts the luminosity of the supernova at maximum. We therefore fit only this period for the lightcurves of the low-redshift supernovae. Similarly, at high redshift the restframe B-band photometry is usually much more densely sampled in time than the restframe V-band data, so we use the stretch factor that best fits the restframe B band data for both low- and high-redshift supernovae, even though at low-redshift the V-band photometry is equally well sampled.

Each supernova peak magnitude was also corrected for Galactic extinction, A_R, using the extinction law of Cardelli, Clayton, & Mathis (1989), first using the color excess, $E(B-V)_{\rm SF\&D}$, at the supernova's Galactic coordinates provided by Schlegel, Finkbeiner, & Davis (1998) and then—for comparison—using the $E(B-V)_{\rm B\&H}$ value provided by Burstein & Heiles (1982, 1998). A_R was calculated from $E(B-V)$ using a value of the total-to-selective extinction ratio, $\mathcal{R}_R \equiv A_R/E(B-V)$, specific to each supernova. These were calculated using the appropriate redshifted supernova spectrum as it would appear through an R-band filter. These values of $\mathcal{R}_R$ range from 2.56 at $z = 0$ to 4.88 at $z = 0.83$. The observed supernova colors were similarly corrected for Galactic extinction. Any extinction in the supernova's host galaxy, or between galaxies, was not corrected for at this stage, but will be analyzed separately in Section 4.

All the same corrections for width-luminosity relation, K corrections, and extinction (but using $\mathcal{R}_B = 4.14$) were applied to the photometry of 18 low-redshift SNe Ia ($z \leq 0.1$) from the Calán/Tololo supernova survey (Hamuy et al. 1996) that were discovered earlier than five days after peak. The lightcurves of these 18 supernovae have all been re-fit since P97, using the more recently available photometry (Hamuy et al. 1996) and our K corrections.

Figures 1 and 2(a) show the Hubble diagram of effective restframe B magnitude corrected for the width-luminosity relation,

$$m_B^{\rm effective} = m_R + \Delta_{\rm corr} - K_{BR} - A_R \qquad (3)$$

as a function of redshift for the 42 Supernova Cosmology Project high-redshift supernovae, along with the 18 Calán/Tololo low-redshift supernovae. (Here, K_{BR} is the cross-filter K correction from observed R band to restframe B band.) Tables 1 and 2 give the corresponding IAU names, redshifts, magnitudes, corrected magnitudes, and their respective uncertainties. As in P97, the inner error bars in Figures 1 and 2 represent the photometric uncertainty, while the outer error bars add in quadrature 0.17 magnitudes of intrinsic dispersion of SN Ia magnitudes that remain after applying the width-luminosity correction. For these plots, the slope of the width-brightness relation was taken to be $\alpha = 0.6$, the best-fit value of Fit C discussed below. (Since both the low- and high-redshift supernova light-curve widths are clustered rather closely around $s = 1$, as shown in Figure 4, the exact choice of α does not change the Hubble diagram significantly.) The theoretical curves for a universe with no cosmological constant are shown as solid lines, for a range of mass density, $\Omega_{\rm M} = 0, 1, 2$. The dashed lines represent alternative flat cosmologies, for which the total mass-energy density $\Omega_{\rm M}+\Omega_\Lambda = 1$ (where $\Omega_\Lambda \equiv \Lambda/3H_0^2$). The range of models shown are for $(\Omega_{\rm M}, \Omega_\Lambda)$ = (0,1), (0.5,0.5), (1,0), which is covered by the matching solid line, and (1.5, –0.5).

3. FITS TO $\Omega_{\rm M}$ AND Ω_Λ

The combined low- and high-redshift supernova datasets of Figure 1 are fit to the Friedman-Robertson-Walker magnitude-redshift relation, expressed as in P97:

$$m_B^{\rm effective} \equiv m_R + \alpha(s-1) - K_{BR} - A_R \qquad (4)$$
$$= \mathcal{M}_B + 5\log \mathcal{D}_L(z; \Omega_{\rm M}, \Omega_\Lambda) \ ,$$

where $\mathcal{D}_L \equiv H_0 d_L$ is the "Hubble-constant-free" luminosity distance and $\mathcal{M}_B \equiv M_B - 5\log H_0 + 25$ is the "Hubble-constant-free" B-band absolute magnitude at maximum of a SN Ia with width s = 1. (These quantities are, respectively, calculated from theory or fit from apparent magnitudes and redshifts, both without any need for H_0. The cosmological-parameter results are thus also completely independent of H_0.) The details of the fitting procedure as presented in P97 were followed, except that both the low- and high-redshift supernovae were fit simultaneously, so that $\mathcal{M}_B$ and α, the slope of the width-luminosity relation, could also be fit in addition to the cosmological parameters $\Omega_{\rm M}$ and Ω_Λ. For most of the analyses in this paper, $\mathcal{M}_B$ and α are statistical "nuisance" parameters; we calculate 2-dimensional confidence regions and single-parameter uncertainties for the cosmological parameters by integrating over these parameters, i.e., $\mathcal{P}(\Omega_{\rm M}, \Omega_\Lambda) = \int\int \mathcal{P}(\Omega_{\rm M}, \Omega_\Lambda, \mathcal{M}_B, \alpha) d\mathcal{M}_B \, d\alpha$.

As in P97, the small correlations between the photometric uncertainties of the high-redshift supernovae, due to shared calibration data, have been accounted for by fitting with a correlation matrix of uncertainties. (The correlation matrix is available at http://www-supernova.lbl.gov.) The low-redshift supernova photometry is more likely to be uncorrelated in its calibration since these supernovae were not discovered in batches. However, we take a 0.01 mag systematic uncertainty in the comparison of the low-redshift B-band photometry and the high-redshift R-band photometry. The stretch-factor uncertainty is propagated with a fixed width-luminosity slope (taken from the low-redshift supernovae; cf. P97), and checked for consistency after the fit.

We have compared the results of Bayesian and classical, "frequentist," fitting procedures. For the Bayesian fits, we have assumed a "prior" probability distribution that has zero probability for $\Omega_{\rm M} < 0$, but otherwise uniform probability in the four parameters $\Omega_{\rm M}$, Ω_Λ, α, and $\mathcal{M}_B$. For the frequentist fits, we have followed the classical statistical procedures described by Feldman & Cousins (1998), to guarantee frequentist coverage of our confidence regions in the physically allowed part of parameter space. Note that throughout the previous cosmology literature, completely unconstrained fits have generally been used that can (and do) lead to confidence regions that include the part of parameter space with negative values for $\Omega_{\rm M}$. The differences between the confidence regions that result from Bayesian and classical analyses are small. We present the Bayesian confidence regions in the figures, since they are somewhat more conservative, i.e. have larger confidence regions, in the vicinity of particular interest near $\Lambda = 0$.

The residual dispersion in SN Ia peak magnitude after correcting for the width-luminosity relation is small, about 0.17 magnitudes, before applying any color-correction. This was reported in Hamuy et al. (1996) for the low-redshift Calan-Tololo supernovae, and it is striking that the same residual is most consistent with the current 42 high-redshift supernovae (see Section 5). It is not clear from the current datasets, however, whether this dispersion is best modeled as a normal distribution (a Gaussian in flux space) or a log-normal distribution (a Gaussian in magnitude space). We have therefore performed the fits two ways: minimizing χ^2 measured using either magnitude residuals or flux residuals. The results are generally in excellent agreement, but since the magnitude fits yield slightly larger confidence regions, we have again chosen this more conservative alternative to report in this paper.

We have analyzed the total set of 60 low- plus high-redshift supernovae in several ways, with the results of each fit presented as a row of Table 3. The most inclusive analyses are presented in the first two rows: Fit A is a fit to the entire dataset, while Fit B excludes two supernovae that are the most significant outliers from the average lightcurve width, s = 1, and two of the remaining supernovae that are the largest residuals from Fit A. Figure 4 shows that the remaining low- and high-redshift supernovae are well matched in their lightcurve width—the error-weighted means are $\langle s \rangle_{\rm Hamuy} = 0.99 \pm 0.01$ and $\langle s \rangle_{\rm SCP} = 1.00 \pm 0.01$—making the results robust with respect to the width-luminosity-relation correction (see Section 4.5). Our primary analysis, Fit C, further excludes two supernovae that are likely to be reddened, and is discussed in the following section.

Fits A and B give very similar results. Removing the two large-residual supernovae from Fit A yields indistinguishable results, while Figure 5(a) shows that the 68% and 90% joint confidence regions for $\Omega_{\rm M}$ and Ω_Λ still change very little after also removing the two supernovae with outlier lightcurve widths. The best-fit mass-density in a flat universe for Fit A is, within a fraction of the uncertainty, the same value as for Fit B, $\Omega_{\rm M}^{\rm flat} = 0.26^{+0.09}_{-0.08}$ (see Table 3). The main difference between the fits is the goodness-of-fit: the larger χ^2 per degree of freedom for Fit A, $\chi^2_\nu = 1.76$, indicates that the outlier supernovae included in this fit are probably not part of a Gaussian distribution and thus will not be appropriately weighted in a χ^2 fit. The χ^2 per degree of freedom for Fit B, $\chi^2_\nu = 1.16$, is over 300 times more probable than that of fit A, and indicates that the remaining 56 supernovae are a reasonable fit to the model, with no large statistical errors remaining unaccounted for.

Of the two large-residual supernovae excluded from the fits after Fit A, one is fainter than the best-fit prediction and one is brighter. The photometric color excess (see Section 4.1) for the fainter supernova, SN 1997O, has an uncertainty that is too large to determine conclusively whether it is reddened. The brighter supernova, SN 1994H, is one of the first seven high-redshift supernovae originally analyzed in P97, and is one of the few supernovae without a spectrum to confirm its classification as a SN Ia. After re-analysis with additional calibration data and improved K-corrections, it remains the brightest outlier in the current sample, but it affects the final cosmological fits much less as one of 42 supernovae, rather than 1 of 5 supernovae in the primary P97 analysis.

4. SYSTEMATIC UNCERTAINTIES AND CROSS-CHECKS

With our large sample of 42 high-redshift SNe, it is not only possible to obtain good statistical uncertainties on the measured parameters, but also to quantify several possible sources of systematic uncertainties. As discussed in P97, the primary approach is to examine subsets of our data that will be affected to lesser extents by the systematic uncertainty being considered. The high-redshift sample is now large enough that these subsets each contain enough supernovae to yield results of high statistical significance.

4.1. *Extragalactic Extinction.*

4.1.1. *Color-Excess Distributions*

Although we have accounted for extinction due to our Galaxy, it is still probable that some supernovae are dimmed by host galaxy dust or intergalactic dust. For a standard dust extinction law (Cardelli, Clayton, & Mathis 1989) the color, B–V, of a supernova will become redder as the amount of extinction, A_B, increases. We thus can look for any extinction differences between the low- and high-redshift supernovae by comparing their restframe colors. Since there is a small dependence of intrinsic color on the lightcurve width, supernova colors can only be compared for the same stretch factor; for a more convenient analysis, we subtract out the intrinsic colors, so that the remaining color excesses can be compared simultaneously for all stretch factors. To determine the restframe color excess $E(B–V)$ for each supernova, we fit the rest-frame B and V photometry to the B and V SN Ia lightcurve templates, with one of the fitting parameters representing the magnitude difference between the two bands at their respective peaks. Note that these lightcurve peaks are $\sim$2 days apart, so the resulting $B_{\rm max}-V_{\rm max}$ color parameter, which is frequently used to describe supernova colors, is not a color measurement on a particular day. The difference of this color parameter from the $B_{\rm max}-V_{\rm max}$ found for a sample of low-redshift supernovae for the same lightcurve stretch-factor (Tripp 1998; Kim et al. 1998; Phillips 1998) does yield the restframe $E(B–V)$ color excess for the fitted supernova.

For the high-redshift supernovae at $0.3 < z < 0.7$, the matching R- and I-band measurements take the place of the restframe B and V measurements and the fit B and V lightcurve templates are K-corrected from the appropriate matching filters, e.g. $R(t) = B(t)+K_{BR}(t)$ (Kim, Goobar, & Perlmutter 1996; Nugent et al. 1998). For the three supernovae at $z > 0.75$, the observed $R-I$ corresponds more closely to a restframe $U-B$ color than to a $B-V$ color, so $E(B-V)$ is calculated from restframe $E(U-B)$ using the extinction law of Cardelli, Clayton, & Mathis (1989). Similarly, for the two SNe Ia at $z \sim 0.18$, $E(B–V)$ is calculated from restframe $E(V–R)$.

Figure 6 shows the color excess distributions for both the low- and high-redshift supernovae, after removing the color excess due to our Galaxy. Six high-redshift supernovae are not shown on this $E(B–V)$ plot, because six of the first seven high-redshift supernovae discovered were not observed in both R and I bands. The color of one low-redshift supernova, SN 1992bc, is poorly determined by the V-band template fit and has also been excluded. Two supernovae in the high-redshift sample are $> 3\sigma$ red-and-faint outliers from the mean in the joint probability distribution of $E(B–V)$ color excess and magnitude residual from Fit B. These two, SNe 1996cg and 1996cn (shown in light shading in Figure 6), are very likely reddened supernovae. To obtain a more robust fit of the cosmological parameters, in Fit C we remove these supernovae from the sample. As can be seen from the Fit-C 68% confidence region of Figure 5(a), these likely-reddened supernovae do not significantly affect any of our results. The main distribution of 38 high-redshift supernovae thus is barely affected by a few reddened events. We find identical results if we exclude the six supernovae without color measurements (Fit G in Table 3). We take Fit C to be our primary analysis for this paper, and in Figure 7, we show a more extensive range of confidence regions for this fit.

4.1.2. *Cross-checks on Extinction*

The color-excess distributions of the Fit C dataset (with the most significant measurements highlighted by dark shading in Figure 6) show no significant difference between the low- and high-redshift means. The dashed curve drawn over the high-redshift distribution of Figure 6 shows the expected distribution if the low-redshift distribution had the measurement uncertainties of the high-redshift supernovae indicated by the dark shading. This shows that the reddening distribution for the high-redshift SNe is consistent with the reddening distribution for the low-redshift SNe, within the measurement uncertainties. The error-weighted means of the low- and high-redshift distributions are almost identical: $\langle E(B–V)\rangle_{\rm Hamuy} = 0.033 \pm 0.014$ mag and $\langle E(B–V)\rangle_{\rm SCP} = 0.035 \pm 0.022$ mag. We also find no significant correlation between the color excess and the statistical weight or redshift of the supernovae within these two redshift ranges.

To test the effect of any remaining high-redshift reddening on the Fit C measurement of the cosmological parameters, we have constructed a Fit H-subset of the high-redshift supernovae that is intentional biased to be bluer than the low-redshift sample. We exclude the error-weighted reddest 25% of the high-redshift supernovae; this excludes 9 high-redshift supernovae with the highest error-weighted $E(B-V)$. We further exclude two supernovae that have large uncertainties in $E(B-V)$ but are significantly faint in their residual from Fit C. This is a somewhat conservative cut since it removes the faintest of the high-redshift supernovae, but it does ensure that the error-weighted $E(B-V)$ mean of the remaining supernova subset is a good indicator of any reddening that could affect the cosmological parameters. The probability that the high-redshift subset of Fit H is redder in the mean than the low-redshift supernovae is less than 5%; This subset is thus very unlikely to be biased to fainter magnitudes by high-redshift reddening. Even with non-standard, "greyer" dust that does not cause as much reddening for the same amount of extinction, a conservative estimate of the probability that the high-redshift subset of Fit H is redder in the mean than the low-redshift supernovae is still less than $\sim$17%, for any high-redshift value of $\mathcal{R}_B \equiv A_B/E(B-V)$ less than twice the low-redshift value. (These same confidence levels are obtained whether using Gaussian statistics, assuming a normal distribution of $E(B-V)$ measurements, or using bootstrap resampling statistics, based on the observed distribution.) The confidence regions of Figure 5(c) and the $\Omega_{\rm M}^{\rm flat}$ results in Table 3 show that the cosmological parameters found for Fit H differ by less than half of a standard deviation from those for Fit C. We take the difference of these fits, 0.03 in $\Omega_{\rm M}^{\rm flat}$ (which corresponds to less than 0.025 in magnitudes) as a $\sim 1\sigma$ upper bound on the systematic uncertainty due to extinction by dust that reddens.

Note that the modes of both distributions appear to be at zero reddening, and similarly the medians of the distributions are quite close to zero reddening: $\langle E(B–V)\rangle_{\rm Hamuy}^{\rm median} = 0.01$ mag and $\langle E(B–V)\rangle_{\rm SCP}^{\rm median} = 0.00$ mag. This should be taken as suggestive rather than conclusive since the zeropoint of the relationship between true color and stretch is not tightly constrained by the current low-redshift SN Ia dataset. This apparent strong clustering of SNe Ia about zero reddening has been noted in the past for low-redshift supernova samples. Proposed explanations have been given based on the relative spatial distributions of the SNe Ia and the dust: Modeling by Hatano, Branch, & Deaton (1997) of the expected extinction of SN Ia disk and bulge populations viewed at random orientations shows an extinction distribution with a strong spiked peak near zero extinction along with a broad, lower-probability wing to higher extinction. This wing will be further suppressed by the observational selection against more reddened SNe, since they are dimmer. (For a flux-limited survey this suppression factor is $10^{-a_R[\mathcal{R}_B E(B-V) - \alpha(s-1)]} \approx 10^{-1.6E(B-V)}$, where a_R is the slope of the supernova number counts.) We also note that the high-redshift supernovae for which we have accurate measurements of apparent separation between SN and host position (generally, those with Hubble Space Telescope imaging) appear to be relatively far from the host center, despite our high search sensitivity to supernovae in front of the host galaxy core (see Pain et al. 1996 for search efficiency studies; also cf. Wang, Höflich, & Wheeler 1997). If generally true for the entire sample, this would be consistent with little extinction.

Our results, however, do not depend on the low- and high-redshift color-excess distributions being consistent with zero reddening. It is only important that the reddening distributions for the low-redshift and high-redshift datasets are statistically the same, and that there is no correlation between reddening and statistical weight in the fit of the cosmological parameters. With both of these conditions satisfied, we find that our measurement of the cosmological parameters is unaffected (to within the statistical error) by any small remaining extinction among the supernovae in the two datasets.

4.1.3. *Analysis with Reddening Correction of Individual Supernovae*

We have also performed fits using restframe B-band magnitudes individually corrected for host galaxy extinction using $A_B = \mathcal{R}_B E(B-V)$ (implicitly assuming that the extragalactic extinction is all at the redshift of the host galaxy). As a direct comparison between the treatment of host galaxy extinction described above and an alternative Bayesian method (Riess, Press, & Kirshner 1996), we applied it to the 53 SNe Ia with color measurements in our Fit C dataset. We find that our cosmological parameter results are robust with respect to this change, although this method can introduce a bias into the extinction corrections, and hence the cosmological parameters. In brief, in this method the Gaussian extinction probability distribution implied by the measured color-excess and its error is multiplied by an assumed *a priori* probability distribution (the Bayesian prior) for the intrinsic distribution of host extinctions. The most probable value of the resulting renormalized probability distribution is taken as the extinction, and following Riess (private communication) the second-moment is taken as the uncertainty. For this analysis, we choose a conservative prior (as given in Riess, Press, & Kirshner 1996) that does not *assume* that the supernovae are unextinguished, but rather is somewhat broader than the true extinction distribution where the majority of the previously observed supernovae apparently suffer very little reddening. (If one alternatively assumes that the current data's extinction distribution is quite as narrow as that of previously observed supernovae, one can choose a less conservative but more realistic narrow prior probability distribution, such as that of Hatano, Branch, & Deaton (1997). This turns out to be quite similar to our previous analysis in Section 4.1.1, since a distribution like that of Hatano, Branch, & Deaton has zero extinction for most supernovae.)

This Bayesian method with a conservative prior will only brighten supernovae, never make them fainter, since it only affects the supernovae with redder measurements than the zero-extinction $E(B-V)$ value, leaving unchanged those measured to be bluer than this. The resulting slight difference between the assumed and true reddening distributions would make no difference in the cosmology measurements if its size were the same at low and high redshifts. However, since the uncertainties, $\sigma_{E(B-V)}^{\mathrm{high}-z}$, in the high-redshift dataset $E(B-V)$ measurements are larger on average than those of the low-redshift dataset, $\sigma_{E(B-V)}^{\mathrm{low}-z}$, this method can over-correct the high-redshift supernovae on average relative to the low-redshift supernovae. Fortunately, as shown in Appendix A, even an extreme case with a true distribution all at zero extinction and a conservative prior would introduce a bias in extinction A_B only of order 0.1 magnitudes at worst for our current low- and high-redshift measurement uncertainties. The results of Fit E are shown in Table 3 and as the dashed contour in Figure 5(d), where it can be seen that compared to Fit C this approach moves the best fit value much less than this, and in the direction expected for this effect (indicated by the arrows in Figure 5d). The fact that $\Omega_{\mathrm{M}}^{\mathrm{flat}}$ changes so little from Case C, even with the possible bias, gives further confidence in the cosmological results.

We can eliminate any such small bias of this method by assuming no Bayesian prior on the host-galaxy extinction, allowing extinction corrections to be negative in the case of supernovae measured to be bluer than the zero-extinction $E(B-V)$ value. As expected, we recover the unbiased results within error, but with larger uncertainties since the Bayesian prior also narrows the error bars in the method of Riess, Press, & Kirshner (1996). However, there remains a potential source of bias when correcting for reddening: the effective ratio of total to selective extinction, $\mathcal{R}_B$, could vary, for several reasons. First, the extinction could be due to host galaxy dust at the supernova's redshift or intergalactic dust at lower redshifts, where it will redden the supernova less since it is acting on a redshifted spectrum. Second, $\mathcal{R}_B$ may be sensitive to dust density, as indicated by variations in the dust extinction laws between various sight-lines in the Galaxy (Clayton & Cardelli 1988; Gordon & Clayton 1998). Changes in metallicity might be expected to be a third possible cause of $\mathcal{R}_B$ evolution, since metallicity is one dust-related quantity known to evolve with redshift (Pettini et al. 1997), but fortunately it appears not to significantly alter $\mathcal{R}_B$ as evidenced by the similarity of the optical portions of the extinction curves of the Galaxy, the LMC, and the SMC (Pei 1992; Gordon & Clayton 1998). Three-filter photometry of high-redshift supernovae currently in progress with the Hubble Space Telescope will help test for such differences in $\mathcal{R}_B$.

To avoid these sources of bias, we consider it important to use and compare both analysis approaches: the rejection of reddened supernovae and the correction of reddened supernovae. We do find consistency in the results calculated both ways. The advantages of the analyses with reddening corrections applied to individual supernovae (with or without a Bayesian prior on host-galaxy extinction) are outweighed by the disadvantages for our sample of high-redshift supernovae; although, in principle, by applying reddening corrections the intrinsic magnitude dispersion of SNe Ia can be reduced from an observed dispersion of 0.17 magnitudes to approximately 0.12 magnitudes, in practice the net improvement for our sample is not significant since uncertainties in the color measurements often dominate. We have therefore chosen for our primary analysis to follow the first procedure discussed above, removing the likely-reddened supernovae (Fit C) and then comparing color-excess means. The systematic difference for Fit H, which rejects the reddest and the faintest high-redshift supernovae, is already quite small, and we avoid introducing additional actual and possible biases. Of course, neither approach avoids biases if $\mathcal{R}_B$ at high redshift is so large $[> 2\mathcal{R}_B(z=0)]$ that dust does not redden the supernovae enough to be distinguished *and* this dust makes more than a few supernovae faint.

4.2. *Malmquist Bias and other Luminosity Biases.*

In the fit of the cosmological parameters to the magnitude-redshift relation, the low-redshift supernova magnitudes primarily determine $\mathcal{M}_B$ and the width-luminosity slope α, and then the comparison with the high-redshift supernova magnitudes primarily determines Ω_M and Ω_Λ. Both low- and high-redshift supernova samples can be biased towards selecting the brighter tail of any distribution in supernova *detection* magnitude for supernovae found near the detection threshold of the search (classical Malmquist bias; Malmquist 1924, 1936). A width-luminosity relation fit to such a biased population would have a slope that is slightly too shallow and a zeropoint slightly too bright. A second bias is also acting on the supernova samples, selecting against supernovae on the narrow-lightcurve side of the width-luminosity relation since such supernovae are detectable for a shorter period of time. Since this bias removes the narrowest/faintest supernova lightcurves preferentially, it culls out the part of the width-brightness distribution most subject to Malmquist bias, and moves the resulting best-fit slope and zeropoint closer to their correct values.

If the Malmquist bias is the same in both datasets, then it is completely absorbed by $\mathcal{M}_B$ and α and does not affect the cosmological parameters. Thus, our principal concern is that there could be a difference in the amount of bias between the low-redshift and high-redshift samples. Note that effects peculiar to photographic SNe searches, such as saturation in galaxy cores, which might in principle select slightly different SNe Ia subpopulations should not be important in determining luminosity bias because lightcurve stretch compensates for any such differences. Moreover, Figure 4 shows that the high-redshift SNe Ia we have discovered have a stretch distribution entirely consistent with those discovered in the Calán/Tololo search.

To estimate the Malmquist bias of the high-redshift-supernova sample, we first determined the completeness of our high-redshift searches as a function of magnitude, through an extensive series of tests inserting artificial SNe into our images (see Pain et al. 1996). We find that roughly 30% of our high-redshift supernovae were detected within twice the SN Ia intrinsic luminosity dispersion of the 50% completeness limit, where the above biases might be important. This is consistent with a simple model where the supernova number counts follow a power-law slope of 0.4 mag^{-1}, similar to that seen for comparably distant galaxies (Smail et al. 1995). For a flux-limited survey of standard candles having the lightcurve-width-corrected luminosity dispersion for SN Ia of $\sim$0.17 mag and this number-count power-law slope, we can calculate that the classical Malmquist bias should be 0.03 mag (see, e.g., Mihalas & Binney 1981, for a derivation of the classical Malmquist bias). (Note that this estimate is much smaller than the Malmquist bias affecting other cosmological distance indicators, due to the much smaller intrinsic luminosity dispersion of SNe Ia.) These high-redshift supernovae, however, are typically detected before maximum, and their detection magnitudes and peak magnitudes have a correlation coefficient of only 0.35, so the effects of classical Malmquist bias should be diluted. Applying the formalism of Willick (1994) we estimate that the decorrelation between detection magnitude and peak magnitude reduces the classical Malmquist bias in the high-redshift sample to only 0.01 mag. The redshift and stretch distributions of the high-redshift supernovae that are near the 50%-completeness limit track those of the overall high-redshift sample, again suggesting that Malmquist biases are small for our dataset.

We cannot make an exactly parallel estimate of Malmquist bias for the low-redshift-supernova sample, because we do not have information for the Calán/Tololo dataset concerning the number of supernovae found near the detection limit. However, the amount of classical Malmquist bias should be similar for the Calán/Tololo SNe since the amount of bias is dominated by the intrinsic luminosity dispersion of SNe Ia, which we find to be the same for the low-redshift and high-redshift samples (see Section 5). Figure 4 shows that the stretch distributions for the high-redshift and low-redshift samples are very similar, so that the compensating effects of stretch-bias should also be similar in the two datasets. The major source of difference in the bias is expected to be due to the close correlation between the detection magnitude and the peak magnitude for the low-redshift supernova search, since this search tended not to find the supernovae as early before peak as the high-redshift search. In addition, the number-counts at low-redshift should be somewhat steeper (Maddox et al. 1990). We thus expect the Calán/Tololo SNe to have a bias closer to that obtained by direct application of the the classical Malmquist bias formula, 0.04 mag. One might also expect "inhomogeneous Malmquist bias" to be more important for the low-redshift supernovae, since in smaller volumes of space inhomogeneities in the host galaxy distribution might by chance put more supernovae near the detection limit than would be expected for a homogeneous distribution. However, after averaging over all the Calán/Tololo supernova-search fields the total low-redshift volume searched is large enough that we expect galaxy count fluctuations of only $\sim$4%, so the classical Malmquist bias is still a good approximation.

We believe that both these low- and high-redshift biases may be smaller, and even closer to each other, due to the mitigating effect of the bias against detection of low-stretch supernovae, discussed above. However, to be conservative, we take the classical Malmquist bias of 0.04 mag for the low-redshift dataset, and the least biased value of 0.01 mag for the high-redshift dataset, and consider systematic uncertainty from this source to be the difference, 0.03 mag, in the direction of low-redshift supernovae more biased than high-redshift. In the other direction, i.e. for high-redshift supernovae more biased than low-redshift, we consider the extreme case of a fortuitously unbiased low-redshift sample, and take the systematic uncertainty bound to be the 0.01 mag bias of the high-redshift sample. (In this direction any systematic error is less relevant to the question of the existence of a cosmological constant.)

4.3. *Gravitational Lensing.*

As discussed in P97, the clumping of mass in the universe could leave the line-of-sight to most of the supernovae underdense, while occasional supernovae may be seen through overdense regions. The latter supernovae could be significantly brightened by gravitational lensing, while the former supernovae would appear somewhat fainter. With enough supernovae, this effect will average out (for inclusive fits, such as Fit A, which include outliers), but the most over-dense lines of sight may be so rare that a set of 42 supernovae may only sample a slightly biased (fainter) set. The probability distribution of these amplifications and deamplifications has previously been studied both analytically and by Monte Carlo simulations. Given the acceptance window of our supernova search, we can integrate the probability distributions from these studies to estimate the bias due to amplified or deamplified supernovae that may be rejected as outliers. This average (de)amplification bias is less than 1% at the redshifts of our supernovae for simulations based on isothermal spheres the size of typical galaxies (Holz & Wald 1998), N-body simulations using realistic mass power spectra (Wambsganss, Cen, & Ostriker 1998), and the analytic models of Frieman (1996).

It is also possible that the small-scale clumping of matter is more extreme, e.g., if significant amounts of mass were in the form of compact objects such as MACHOs. This could lead to many supernova sightlines that are not just under-dense, but nearly empty. Once again, only the very rare line of sight would have a compact object in it, amplifying the supernova signal. To first approximation, with 42 supernovae we would see only the nearly empty beams, and thus only deamplifications. The appropriate luminosity-distance formula in this case is not the Friedmann-Robertson-Walker (FRW) formula but rather the "partially filled beam" formula with a mass filling factor, $\eta \approx 0$ (see Kantowski 1998, and references therein). We present the results of the fit of our data (Fit K) with this luminosity-distance formula (as calculated using the code of Kayser, Helbig, & Schramm 1996) in Figure 8. A more realistic limit on this point-like mass density can be estimated, because we would expect such point-like masses to collect into the gravitational potential wells already marked by galaxies and clusters. Fukugita, Hogan, & Peebles (1997) estimate an upper limit of $\Omega_{\rm M} < 0.25$ on the mass which is clustered like galaxies. In Figure 8, we also show the confidence region from Fit L, assuming that only the mass density contribution up to $\Omega_{\rm M} = 0.25$ is point-like, with filling factor $\eta = 0$, and that η rises to 0.75 at $\Omega_{\rm M} = 1$. We see that at low mass density, the Friedman-Robertson-Walker fit is already very close to the nearly empty-beam ($\eta \approx 0$) scenario, so the results are quite similar. At high mass density, the results diverge, although only minimally for Fit L; the best fit in a flat universe is $\Omega_{\rm M}^{\rm flat} = 0.34^{+0.10}_{-0.09}$.

4.4. *Supernova Evolution and Progenitor Environment Evolution*

The spectrum of a SN Ia on any given point in its lightcurve reflects the complex physical state of the supernova on that day: the distribution, abundances, excitations, and velocities of the elements that the photons encounter as they leave the expanding photosphere all imprint on the spectra. So far, the high-redshift supernovae that have been studied have lightcurve shapes just like those of low-redshift supernovae (see Goldhaber et al. 1998), and their spectra show the same features on the same day of the lightcurve as their low-redshift counterparts having comparable lightcurve width. This is true all the way out to the $z = 0.83$ limit of the current sample (Perlmutter et al. 1998b). We take this as a strong indication that the physical parameters of the supernova explosions are not evolving significantly over this time span.

Theoretically, evolutionary effects might be caused by changes in progenitor populations or environments. For example, lower metallicity and more massive SN Ia-progenitor binary systems should be found in younger stellar populations. For the redshifts that we are considering, $z < 0.85$, the change in average progenitor masses may be small (Ruiz-Lapuente, Canal, & Burkert 1997; Ruiz-Lapuente 1998). However, such progenitor mass differences or differences in typical progenitor metallicity are expected to lead to differences in the final C/O ratio in the exploding white dwarf, and hence affect the energetics of the explosion. The primary concern here would be if this changed the zero-point of the width-luminosity relation. We can look for such changes by comparing lightcurve rise times between low and high-redshift supernova samples, since this is a sensitive indicator of explosion energetics. Preliminary indications suggest that no significant rise-time change is seen, with an upper limit of $\lesssim 1$ day for our sample (see forthcoming high-redshift studies of Goldhaber et al. 1998 and Nugent et al. 1998, and low-redshift bounds from Vacca & Leibundgut 1996, Leibundgut et al. 1996b, and Marvin & Perlmutter 1989). This tight a constraint on rise-time change would theoretically limit the zero-point change to less than $\sim$0.1 mag (see Nugent et al. 1995; Höflich, Wheeler, & Thielemann 1998).

A change in typical C/O ratio can also affect the ignition density of the explosion and the propagation characteristics of the burning front. Such changes would be expected to appear as differences in lightcurve timescales before and after maximum (Höflich & Khokhlov 1996). Preliminary indications of consistency between such low- and high-redshift lightcurve timescales suggest that this is probably not a major effect for our supernova samples (Goldhaber et al., 1998).

Changes in typical progenitor metallicity should also directly cause some differences in SN Ia spectral features (Höflich, Wheeler, & Thielemann 1998). Spectral differences big enough to affect the B and V-band lightcurves (see, for example, the extreme mixing models presented in Figure 9 of Höflich, Wheeler, & Thielemann 1998) should be clearly visible for the best signal-to-noise spectra we have obtained for our distant supernovae, yet they are not seen (Filippenko et al. 1998; Hook, Nugent, et al., 1998). The consistency of slopes in the lightcurve width-luminosity relation for the low- and high-redshift supernovae can also constrain the possibility of a strong metallicity effect of the type that Höflich, Wheeler, & Thielemann (1998) describes.

An additional concern might be that even small changes in spectral features with metallicity could in turn affect the calculations of K corrections and reddening corrections. This effect, too, is very small, less than 0.01 magnitudes, for photometric observations of SNe Ia conducted in the restframe B or V bands (see Figures 8 and 10 of Höflich, Wheeler, & Thielemann 1998), as is the case for almost all of our supernovae. (Only two of our supernovae have primary observations that are sensitive to the restframe U band, where the magnitude can change by $\sim$0.05 magnitudes, and these are the two supernovae with the lowest weights in our fits, as shown by the error bars of Figures 2. In general the I-band observations, which are mostly sensitive to the restframe B band, provide the primary lightcurve at redshifts above 0.7.)

The above analyses constrain only the effect of progenitor-environment evolution on SN Ia intrinsic luminosity; however, the extinction of the supernova light could also be affected, if the amount or character of the dust evolves, e.g. with host galaxy age. In Section 4.1, we limited the size of this extinction evolution for dust that reddens, but evolution of "grey" dust grains larger than $\sim 0.1\mu$m, which would cause more color-neutral optical extinction, can evade these color measurements. The following two analysis approaches can constrain both evolution effects, intrinsic SN Ia luminosity evolution and extinction evolution. They take advantage of the fact that galaxy properties such as formation age, star-formation history, and metallicity are not monotonic functions of redshift, so even the low-redshift SNe Ia are found in galaxies with a wide range of ages and metallicities. It is a shift in the *distribution* of relevant host-galaxy properties occurring between $z \sim 0$ and $z \sim 0.5$ that could cause any evolutionary effects.

Width-Luminosity Relation Across Low-Redshift Environments. To the extent that low-redshift SNe Ia arise from progenitors with a range of metallicities and ages, the lightcurve width-luminosity relation discovered for these SNe can already account for these effects (cf. Hamuy et al. 1995, 1996). When corrected for the width-luminosity relation, the peak magnitudes of low-redshift SNe Ia exhibit a very narrow magnitude dispersion about the Hubble line, with no evidence of a significant progenitor-environment difference in the residuals from this fit. It therefore does not matter if the population of progenitors evolves such that the measured lightcurve widths change, since the width-luminosity relation apparently is able to correct for these changes. It will be important to continue to study further nearby SNe Ia to test this conclusion with as wide a range of host-galaxy ages and metallicities as possible.

Matching Low- and High-Redshift Environments. Galaxies with different morphological classifications result from different evolutionary histories. To the extent that galaxies with similar classifications have similar histories, we can also check for evolutionary effects by using supernovae in our cosmology measurements with matching host galaxy classifications. If the same cosmological results are found for each measurement based on a subset of low- and high-redshift supernovae sharing a given host-galaxy classification, we can rule out many evolutionary scenarios. In the simplest such test, we compare the cosmological parameters measured from low- and high-redshift elliptical host galaxies with those measured from low- and high-redshift spiral host galaxies. Without high-resolution host-galaxy images for most of our high-redshift sample, we currently can only approximate this test for the smaller number of supernovae for which the host-galaxy spectrum gives a strong indication of galaxy classification. The resulting sets of 9 elliptical-host and 8 spiral-host high-redshift supernovae are matched to the 4 elliptical-host and 10 spiral-host low-redshift supernovae (based on the morphological classifications listed in Hamuy et al. 1996, and excluding two with SB0 hosts). We find no significant change in the best-fit cosmology for the elliptical host-galaxy subset (with both the low- and high-redshift subsets about one sigma brighter than the mean of the full sets), and a small ($<1\sigma$) shift lower in $\Omega_M^{\rm flat}$ for the spiral host-galaxy subset. Although the consistency of these subset results is encouraging, the uncertainties are still large enough (approximately twice the Fit C uncertainties) that this test will need to await the host-galaxy classification of the full set of high-redshift supernovae and a larger low-redshift supernova sample.

4.5. *Further Cross-Checks*

We have checked several other possible effects that might bias our results, by fitting different supernova subsets and using alternative analyses:

Sensitivity to Width-Luminosity Correction. Although the lightcurve width correction provides some insurance against supernova evolution biasing our results, Figure 4 shows that almost all of the Fit C supernovae at both low- and high-redshift are clustered tightly around the most-probable value of $s = 1$, the standard width for a B-band Leibundgut SN Ia template lightcurve. Our results are therefore rather robust with respect to the actual choice of width-luminosity relation. We have tested this sensitivity by re-fitting the supernovae of Fit C, but with no width-luminosity correction. The results (Fit D), as shown in Figure 5(b), and listed in Table 3, are in extremely close agreement with those of the lightcurve-width-corrected Fit C. The statistical uncertainties are also quite close; the lightcurve-width correction does not significantly improve the statistical dispersion for the magnitude residuals, because of the uncertainty in s, the measured lightcurve width. It is clear that the best-fit cosmology does not depend strongly on the extra degree of freedom allowed by including the width-luminosity relation in the fit.

Sensitivity to Non-SN Ia Contamination. We have tested for the possibility of contamination by non-SN Ia events masquerading as SNe Ia in our sample, by performing a fit after excluding any supernovae with less certain SN Ia spectroscopic and photometric identification. This selection removes the large statistical outliers from the sample. In part, this may be because the host-galaxy contamination that can make it difficult to identify the supernova spectrum can also increase the odds of extinction or other systematic uncertainties in photometry. For this more “pure” sample of 43 supernovae, we find $\Omega_M^{\rm flat} = 0.33^{+0.10}_{-0.09}$, just over half of a standard deviation from Fit C.

Sensitivity to Galactic Extinction Model. Finally, we have tested the effect of the choice of Galactic extinction model, with a fit using the model of Burstein & Heiles (1982), rather than Schlegel, Finkbeiner, & Davis (1998). We find no significant difference in the best-fit cosmological parameters, although we note that the extinction near the Galactic pole is somewhat larger in the Schlegel, Finkbeiner, & Davis model and this leads to a $\sim$0.03 magnitude larger average offset between the low-redshift supernova B-band observations and the high-redshift supernovae R-band observations.

5. RESULTS AND ERROR BUDGET

From Table 3 and Figure 5(a), it is clear that the results of Fits A, B, and C are quite close to each other, so we can conclude that our measurement is robust with respect to the choice of these supernova subsets. The inclusive Fits A and B are the fits with the least subjective selection of the data. They already indicate the main cosmological results from this dataset. However, to make our results robust with respect to host-galaxy reddening, we use Fit C as our primary fit in this paper. For Fit C, we find $\Omega_M^{\rm flat} = 0.28^{+0.09}_{-0.08}$ in a flat universe. Cosmologies with $\Omega_\Lambda = 0$ are a poor fit to the data, at the 99.8% confidence level. The contours of Figure 7 more fully characterize the best-fit confidence regions. (The table of this two-dimensional probability distribution is available at http://www-supernova.lbl.gov/.)

The residual plots of Figure 2(b and c) indicate that the best-fit $\Omega_M^{\rm flat}$ in a flat universe is consistent across the redshift range of the high-redshift supernovae. Figure 2(c) shows the residuals normalized by uncertainties; their scatter can be seen to be typical of a normal-distributed variable, with the exception of the two outlier supernovae that are removed from all fits after Fit A, as discussed above. Figure 3 compares the magnitude-residual distributions (the projections of Figure 2b) to the Gaussian distributions expected given the measurement uncertainties and an intrinsic dispersion of 0.17 mag. Both the low- and high-redshift distributions are consistent with the expected distributions; the formal calculation of the SN Ia intrinsic-dispersion component of the observed magnitude dispersion ($\sigma^2_{\rm intrinsic} = \sigma^2_{\rm observed} - \sigma^2_{\rm measurement}$) yields $\sigma_{\rm intrinsic} = 0.154 \pm 0.04$ for the low-redshift distribution and $\sigma_{\rm intrinsic} = 0.157 \pm 0.025$ for the high-redshift distribution. The χ^2 per degree of freedom for this fit, $\chi^2_\nu = 1.12$, also indicates that the fit model is a reasonable description of the data. The narrow intrinsic dispersion—which does not increase at high redshift—provides additional evidence against an increase in extinction with redshift. Even if there is grey dust that dims the supernovae without reddening them, the dispersion would increase, unless the dust is distributed very uniformly.

A flat, $\Omega_\Lambda = 0$ cosmology is a quite poor fit to the data. The $(\Omega_{\rm M}, \Omega_\Lambda) = (1, 0)$ line on Figure 2(b) shows that 38 out of 42 high-redshift supernovae are fainter than predicted for this model. These supernovae would have to be over 0.4 magnitudes brighter than measured (or the low-redshift supernovae 0.4 magnitudes fainter) for this model to fit the data.

The $(\Omega_{\rm M}, \Omega_\Lambda) = (0, 0)$ upper solid line on Figure 2(a) shows that the data are still not a good fit to an "empty universe," with zero mass density and cosmological constant. The high-redshift supernovae are as a group fainter than predicted for this cosmology; in this case, these supernovae would have to be almost 0.15 magnitudes brighter for this empty cosmology to fit the data, and the discrepancy is even larger for $\Omega_{\rm M} > 0$. This is reflected in the high probability (99.8%) of $\Omega_\Lambda > 0$.

As discussed in Goobar & Perlmutter (1995), the slope of the contours in Figure 7 is a function of the supernova redshift distribution; since most of the supernovae reported here are near $z \sim 0.5$, the confidence region is approximately fit by $0.8\,\Omega_{\rm M} - 0.6\,\Omega_\Lambda \approx -0.2 \pm 0.1$. (The orthogonal linear combination, which is poorly constrained, is fit by $0.6\,\Omega_{\rm M} + 0.8\,\Omega_\Lambda \approx 1.5 \pm 0.7$.) In P97, we emphasized that the well-constrained linear combination is not parallel to any contour of constant current-deceleration-parameter, $q_0 = \Omega_{\rm M}/2 - \Omega_\Lambda$; the accelerating/decelerating universe line of Figure 9 shows one such contour at $q_0 = 0$. Note that with almost all of the confidence region above this line, only currently accelerating universes fit the data well. As more of our highest redshift supernovae are analyzed, the long dimension of the confidence region will shorten.

Error Budget

Most of the sources of statistical error contribute a statistical uncertainty to each supernova individually, and are included in the uncertainties listed in Tables 1 and 2, with small correlations between these uncertainties given in the correlated-error matrices (available at http://www-supernova.lbl.gov). These supernova-specific statistical uncertainties include the measurement errors on SN peak magnitude, lightcurve stretch factor, and absolute photometric calibration. The two sources of statistical error that are common to all the supernovae are the intrinsic dispersion of SN Ia luminosities after correcting for the width-luminosity relation, taken as 0.17 mag, and the redshift uncertainty due to peculiar velocities, which are taken as 300 km s^{-1}. Note that the statistical error in $\mathcal{M}_B$ and α are derived quantities from our four-parameter fits. By integrating the four-dimensional probability distributions over these two variables, their uncertainties are included in the final statistical errors.

All uncertainties that are not included in the statistical error budget are treated as systematic errors for the purposes of this paper. In Sections 2 and 4, we have identified and bounded four potentially significant sources of systematic uncertainty: (1) the extinction uncertainty for dust that reddens, bounded at $<$0.025 magnitudes, the maximal effect of the nine reddest and two faintest of the high-redshift supernovae; (2) the difference between the Malmquist bias of the low- and high-redshift supernovae, bounded at $\leq$0.03 magnitudes for low-redshift supernovae biased intrinsically brighter than high-redshift supernovae, and $<$0.01 magnitudes for high-redshift supernovae biased brighter than low-redshift supernovae; (3) the cross-filter K-correction uncertainty of $<$0.02 magnitudes; and (4) the $<$0.01 magnitudes uncertainty in K corrections and reddening corrections due to the effect of progenitor metallicity evolution on the rest-frame B-band spectral features. We take the total identified systematic uncertainty to be the quadrature sum of the sources: +0.04 magnitudes in the direction of spuriously fainter high-redshift or brighter low-redshift supernovae, and –0.03 magnitudes in the opposite direction.

Note that we treat the possibility of gravitational lensing due to small-scale clumping of mass as a separate analysis case, rather than as a contributing systematic error in our primary analysis; the total systematic uncertainty applies to this analysis as well. There are also several more hypothetical sources of systematic error discussed in Section 4, which are not included in our calculation of identified systematics. These include grey dust [with $\mathcal{R}_B(z=0.5) > 2\mathcal{R}_B(z=0)$] and any SN Ia evolutionary effects that might change the zero point of the lightcurve width-luminosity relation. We have presented bounds and tests for these effects which give preliminary indications that they are not large sources of uncertainty, but at this time they remain difficult to quantify, at least partly because the proposed physical processes and entities that might cause the effects are not completely defined.

To characterize the effect of the identified systematic uncertainties, we have refit the supernovae of Fit C for the hypothetical case (Fit J) in which each of the high-redshift supernovae were discovered to be 0.04 magnitudes brighter than measured, or, equivalently, the low-redshift supernovae were discovered to be 0.04 magnitudes fainter than measured. Figure 5(e) and Table 3 show the results of this fit. The best-fit flat-universe $\Omega_{\rm M}^{\rm flat}$ varies from that of Fit C by 0.05, less than the statistical error bar. The probability of $\Omega_\Lambda > 0$ is still over 99%. When we fit with the smaller systematic error in the opposite direction (i.e., high-redshift supernovae discovered to be 0.03 magnitudes fainter than measured), we find (Fit I) only a 0.04 shift in $\Omega_{\rm M}^{\rm flat}$ from Fit C.

The measurement error of the cosmological parameters has contributions from both the low- and high-redshift supernova datasets. To identify the approximate relative importance of these two contributory sources, we reanalyzed the Fit C dataset, first fitting $\mathcal{M}_B$ and α to the low-redshift dataset (this is relatively insensitive to cosmological model), and then fitting $\Omega_{\rm M}$ and Ω_Λ to the high-redshift dataset. (This is only an approximation, since it neglects the small influence of the low-redshift supernovae on $\Omega_{\rm M}$ and Ω_Λ, and of the high-redshift supernovae on $\mathcal{M}_B$ and α, in the standard four-parameter fit.) Figure 5(f) shows this $\Omega_{\rm M}$–Ω_Λ fit as a solid contour (labeled Fit M), with the 1-sigma uncertainties on $\mathcal{M}_B$ and α included with the systematic uncertainties in the dashed-line confidence contours. This approach parallels the analyses of Perlmutter et al. (1997e, 1998c, 1998b), and thus also provides a direct comparison with the earlier results. We find that the more important contribution to the uncertainty is currently due to the low-redshift supernova sample. If three times as many well-observed low-redshift supernovae were discovered and included in the analysis, then the statistical uncertainty from the low-redshift dataset would be smaller than the other sources of uncertainty.

We summarize the relative statistical and systematic uncertainty contributions in Table 4.

6. CONCLUSIONS AND DISCUSSION

The confidence regions of Figure 7 and the residual plot of Figure 2(b) lead to several striking implications. First, the data are strongly inconsistent with the $\Lambda = 0$, flat universe model (indicated with a circle) that has been the theoretically favored cosmology. If the simplest inflationary theories are correct and the universe is spatially flat, then the supernova data imply that there is a significant, positive cosmological constant. Thus, the universe may be flat, *or* there may be little or no cosmological constant, but the data are not consistent with both possibilities simultaneously. This is the most unambiguous result of the current dataset.

Second, this dataset directly addresses the age of the universe relative to the Hubble time, H_0^{-1}. Figure 9 shows that the Ω_M–Ω_Λ confidence regions are almost parallel to contours of constant age. For any value of the Hubble constant less than $H_0 = 70$ km s^{-1} Mpc^{-1}, the implied age of the universe is greater than 13 Gyr, allowing enough time for the oldest stars in globular clusters to evolve (Chaboyer et al. 1998; Gratton et al. 1997). Integrating over Ω_M and Ω_Λ, the best fit value of the age in Hubble-time units is $H_0 t_0 = 0.93^{+0.06}_{-0.06}$ or equivalently $t_0 = 14.5^{+1.0}_{-1.0}(0.63/h)$ Gyr. The age would be somewhat larger in a flat universe: $H_0 t_0^{\rm flat} = 0.96^{+0.09}_{-0.07}$ or equivalently $t_0^{\rm flat} = 14.9^{+1.4}_{-1.1}(0.63/h)$ Gyr.

Third, even if the universe is not flat, the confidence regions of Figure 7 suggest that the cosmological constant is a significant constituent of the energy density of the universe. The best-fit model (the center of the shaded contours) indicates that the energy density in the cosmological constant is $\sim$0.5 more than that in the form of mass energy density. All of the alternative fits listed in Table 3 indicate a positive cosmological constant with confidence levels of order 99%, even with the systematic uncertainty included in the fit or with a clumped-matter metric.

Given the potentially revolutionary nature of this third conclusion, it is important to reexamine the evidence carefully to find possible loopholes. None of the identified sources of statistical and systematic uncertainty described in the previous sections could account for the data in a $\Lambda = 0$ universe. If the universe does in fact have zero cosmological constant, then some additional physical effect or "conspiracy" of statistical effects must be operative—and must make the high-redshift supernovae appear almost 0.15 mag ($\sim$15% in flux) fainter than the low-redshift supernovae. At this stage in the study of SNe Ia, we consider this unlikely but not impossible. For example, as mentioned above, some carefully constructed smooth distribution of large-grain-size grey dust that evolves similarly for elliptical and spiral galaxies could evade our current tests. Also, the full dataset of well-studied SNe Ia is still relatively small, particularly at low redshifts, and we would like to see a more extensive study of SNe Ia in many different host-galaxy environments before we consider all plausible loopholes (including those listed in Table 4B) to be closed.

Many of these residual concerns about the measurement can be addressed with new studies of low-redshift supernovae. Larger samples of well-studied low-redshift supernovae will permit detailed analyses of statistically significant SN Ia subsamples in differing host environments. For example, the width-luminosity relation can be checked and compared for supernovae in elliptical host galaxies, in the cores of spiral galaxies, and in the outskirts of spiral galaxies. This comparison can mimic the effects of finding high-redshift supernovae with a range of progenitor ages, metallicities, etc. So far, the results of such studies with small statistics has not shown any difference in width-luminosity relation for this range of environments. These empirical tests of the SNe Ia can also be complemented by better theoretical models. As the datasets improve, we can expect to learn more about the physics of SN Ia explosions and their dependence on the progenitor environment, strengthening the confidence in the empirical calibrations. Finally, new well-controlled, digital searches for SNe Ia at low redshift will also be able to further reduce the uncertainties due to systematics such as Malmquist bias.

6.1. *Comparison with Previous Results*

A comparison with the first supernova measurement of the cosmological parameters in P97 highlights an important aspect of the current measurement. As discussed in Section 3, the P97 measurement was strongly skewed by SN 1994H, one of the two supernovae that are clear statistical outliers from the current 42-supernova distribution. If SN 1994H had not been included in the P97 sample, then the cosmological measurements would have agreed within the 1σ error bars with the current result. (The small changes in the K-corrections discussed in Section 2 are not a significant factor in arriving at this agreement.) With the small P97 sample size of seven supernovae (only five of which were used in the P97 width-corrected analysis), and somewhat larger measurement uncertainties, it was not possible to distinguish SN 1994H as the statistical outlier. It is only with the much larger current sample size that it is easy to distinguish such outliers on a graph such as Figure 2(c).

The fact that there are any outliers at all raises one cautionary flag for the current measurement. Although neither of the current two outliers is a clearly aberrant SN Ia (one has no SN Ia spectral confirmation and the other has a relatively poor constraint on host-galaxy extinction), we are watching carefully for such aberrant events in future low- and high-redshift datasets. Ideally, the one-parameter width-luminosity relationship for SNe Ia would completely account for every single well-studied SN Ia event. This is not a requirement for a robust measurement, but any exceptions that are discovered would provide an indicator of as-yet undetected parameters within the main SN Ia distribution.

Our first presentation of the cosmological parameter measurement (Perlmutter et al. 1998c), based on 40 of the current 42 high-redshift supernovae, found the same basic results as the current analysis: A flat universe was shown to require a cosmological constant, and only a small region of low-mass-density parameter space, with all the systematic uncertainty included, could allow for $\Lambda = 0$. (Fit M of Figure 5(f) still shows almost the same confidence region, with the same analysis approach). The current confidence region of Figure 7 has changed very little from the corresponding confidence region of Perlmutter et al. (1998c), but since most of the uncertainties in the low-redshift dataset are now included in the statistical error, the remaining systematic error is now a small part of the error budget.

The more recent analysis of 16 high-redshift supernovae by Riess et al. (1998) also show a very similar Ω_M-Ω_Λ confidence region. The best fits for mass density in a flat-universe are $\Omega_M^{\rm flat} = 0.28 \pm 0.10$ or $\Omega_M^{\rm flat} = 0.16 \pm 0.09$ for the two alternative analyses of their 9 independent, well-observed, spectroscopically-confirmed supernovae. The best fits for the age of the universe for these analyses are $H_0t_0 = 0.90^{+0.07}_{-0.05}$ and $H_0t_0 = 0.98^{+0.07}_{-0.05}$. To first order, the Riess et al. result provides an important independent cross-check for all three conclusions discussed above, since it was based on a separate high-redshift supernova search and analysis chain (see Schmidt et al. 1998). One caveat, however, is that their Ω_M-Ω_Λ confidence-region result cannot be directly compared to ours to check for independent consistency, because the low-redshift-supernova datasets are not independent: a large fraction of these supernovae with the highest weight in both analyses are from the Calán/Tololo Supernova Survey (which provided many well-measured supernovae that were far enough into the Hubble flow so that their peculiar velocities added negligible redshift-uncertainty). Moreover, two of the 16 high-redshift supernovae included in the Riess et al. confidence-region analyses were from our sample of 42 Supernova Cosmology Project supernovae; Riess et al. included them with an alternative analysis technique applied to a subset of our photometry results. (In particular, their result uses the highest-redshift supernova from our 42-supernova sample, which has strong weight in our analysis due to the excellent Hubble Space Telescope photometry.) Finally, although the analysis techniques are mostly independent, the *K* corrections are based on the same Nugent et al. (1998) approach discussed above.

6.2. *Comparison with Complementary Constraints on Ω_M and Ω_Λ*

Significant progress is being made in the measurement of the cosmological parameters using complementary techniques that are sensitive to different linear combinations of Ω_M and Ω_Λ, and have different potential systematics or model dependencies. Dynamical methods, for example, are particularly sensitive to Ω_M, since Ω_Λ affects dynamics only weakly. Since there is evidence that dynamical estimates of Ω_M depend on scale, the most appropriate measures to compare with our result are those obtained on large scales. From the abundance—indeed the mere existence—of rich clusters at high redshift, Bahcall & Fan (1998) find $\Omega_M = 0.2^{+0.3}_{-0.1}$ (95% confidence). The CNOC collaboration (Carlberg et al. 1996, 1998) apply evolution-corrected mass-to-light ratios determined from virial mass estimates of X-ray clusters to the luminosity density of the universe and find $\Omega_M = 0.17 \pm 0.07$ for $\Omega_\Lambda = 0$ ($\sim$90% confidence), with small changes in these results for different values of Ω_Λ (cf. Carlberg 1997). Detailed studies of the peculiar velocities of galaxies (e.g., Willick et al. 1997; Willick & Strauss 1998; Riess et al. 1997b; but see Sigad et al. 1998) are now giving estimates of $\beta = \Omega_M^{0.6}/b_{\rm IRAS} \approx 0.45 \pm 0.11$ (95% confidence)[1], where b is the ratio of density contrast in galaxies compared to that in all matter. Under the simplest assumption of no large-scale biasing for IRAS galaxies, $b = 1$, these results give $\Omega_M \approx 0.26 \pm 0.11$ (95% confidence), in agreement with the other dynamical estimates—and with our supernova results for a flat cosmology.

A form of the angular-size distance cosmological test has been developed in a series of papers (cf. Guerra & Daly 1998, and references therein) and implemented for a sample of fourteen radio galaxies by Daly, Guerra, & Wan (1998). The method uses the mean observed separation of the radio lobes compared to a canonical maximum lobe size—calculated from the inferred magnetic field strength, lobe propagation velocity, and lobe width—as a calibrated standard ruler. The confidence region in the Ω_M–Ω_Λ plane shown in Daly, Guerra, & Wan (1998) is in broad agreement with the SN Ia results we report; they find $\Omega_M = 0.2^{+0.3}_{-0.2}$ (68% confidence) for a flat cosmology.

QSO gravitational lensing statistics are dependent on both volume and relative distances, and thus are more sensitive to Ω_Λ. Using gravitational lensing statistics, Kochanek (1996) finds $\Omega_\Lambda < 0.66$ (at 95% confidence for $\Omega_M + \Omega_\Lambda = 1$), and $\Omega_M > 0.15$. Falco, Kochanek, & Munoz (1998) obtained further information on the redshift distribution of radio sources which allows calculation of the absolute lensing probability for both optical and radio lenses. Formally their 90% confidence levels in the Ω_M–Ω_Λ plane have no overlap with those we report here. However, as Falco, Kochanek, & Munoz (1998) discuss, these results do depend on the choice of galaxy sub-type luminosity functions in the lens models. Chiba & Yoshii (1998) emphasized this point, reporting an analysis with E/S0 luminosity functions that yielded a best-fit mass density in a flat cosmology of $\Omega_M^{\rm flat} = 0.3^{+0.2}_{-0.1}$, in agreement with our SN Ia results.

Several papers have emphasized that upcoming balloon and satellite studies of the Cosmic Background Radiation (CBR) should provide a good measurement of the sum of the energy densities, $\Omega_M + \Omega_\Lambda$, and thus provide almost orthogonal information to the supernova measurements (White 1998; Tegmark et al. 1998). In particular, the position of the first acoustic peak in the CBR power spectrum is sensitive to this combination of the cosmological parameters. The current results, while not conclusive, are already somewhat inconsistent with over-closed ($\Omega_M + \Omega_\Lambda >> 1$) cosmologies and "near-empty" ($\Omega_M + \Omega_\Lambda \lesssim 0.4$) cosmologies, and may exclude the upper right and lower left regions of Figure 7 (see, e.g., Lineweaver 1998; Efstathiou et al. 1998).

6.3. *Cosmological Implications*

If, in fact, the universe has a dominant energy contribution from a cosmological constant, there are two coincidences that must be addressed in future cosmological theories. First, a cosmological constant in the range shown in Figure 7 corresponds to a very small energy density relative to the vacuum-energy-density scale of particle-physics energy zero-points (see Carroll, Press, & Turner 1992, for a discussion of this point). Previously, this had been seen as an argument for a zero cosmological constant, since presumably some symmetry of the particle-physics model is causing cancelations of this vacuum energy density. Now, it would be necessary to explain how this value comes to be so small, yet non-zero.

Second, there is the coincidence that the cosmological constant value is comparable to the current mass-energy density. As the universe expands, the matter energy density falls as the third power of the scale, while the cosmological constant remains unchanged. One therefore would require initial conditions in which the ratio of densities is a special, infinitesimal value of order 10^{-100} in order for the two densities to coincide today. (The cross-over between mass-dominated and Λ-dominated energy density occurred at $z \approx 0.37$, for a flat $\Omega_M \approx 0.28$ universe, whereas the cross-over between deceleration and acceleration occurred when $(1+z)^3\Omega_M/2 = \Omega_\Lambda$, that is at $z \approx 0.73$. This was approximately when SN 1997G exploded, over 6 billion years ago.)

It has been suggested that these cosmological coincidences could be explained if the magnitude-redshift relation we find for SNe Ia is due not to a cosmological constant, but rather to

[1]This is an error-weighted mean of Willick et al. (1997) and Riess et al. (1997b), with optical results converted to equivalent IRAS results using $b_{\rm Opt}/b_{\rm IRAS} = 1.20 \pm 0.05$ from Oliver et al. (1996).

a different, previously unknown physical entity that contributes to the universe's total energy density (see, e.g., Steinhardt 1996; Turner & White 1997; Caldwell, Dave, & Steinhardt 1998). Such an entity can lead to a different expansion history than the cosmological constant does, because it can have a different relation ("equation of state") between its density ρ and pressure p than that of the cosmological constant, $p_\Lambda/\rho_\Lambda = -1$. We can obtain constraints on this equation-of-state ratio, $w \equiv p/\rho$, and check for consistency with alternative theories (including the cosmological constant with $w = -1$) by fitting the alternative expansion histories to data; White (1998) has discussed such constraints from earlier supernovae and CBR results. In Figure 10, we update these constraints for our current supernova dataset, for the simplest case of a flat universe and an equation of state that does not vary in time (cf. Garnavich et al. 1998b, for comparison with their high-redshift supernova dataset, and Aldering et al. 1998 for time-varying equations of state fit to our dataset). In this simple case, a cosmological-constant equation of state can fit our data if the mass density is in the range $0.2 \lesssim \Omega_M \lesssim 0.4$. However, all the cosmological models shown in Figure 10 still require that the initial conditions for the new energy density be tuned with extreme precision to reach their current-day values. Zlatev, Wang, & Steinhardt (1998) have shown that some time-varying-w theories naturally channel the new energy density term to "track" the matter term, as the universe expands, leading—without coincidences—to values of an effective vacuum energy density today that are comparable to the mass energy density. These models require $w \gtrsim -0.8$ at all times up to the present, for $\Omega_M \geq 0.2$. The supernova dataset presented here and future complementary datasets will allow us to explore these possibilities.

The observations described in this paper were primarily obtained as visiting/guest astronomers at the Cerro Tololo Inter-American Observatory 4-meter telescope, operated by the National Optical Astronomy Observatory under contract to the National Science Foundation; the Keck I and II 10-m telescopes of the California Association for Research in Astronomy; the Wisconsin-Indiana-Yale-NOAO (WIYN) telescope; the European Southern Observatory 3.6-meter telescope; the Isaac Newton and William Herschel Telescopes, operated by the Royal Greenwich Observatory at the Spanish Observatorio del Roque de los Muchachos of the Instituto de Astrofisica de Canarias; the Hubble Space Telescope, and the Nordic Optical 2.5-meter telescope. We thank the dedicated staff of these observatories for their excellent assistance in pursuit of this project. In particular, Dianne Harmer, Paul Smith and Daryl Willmarth were extraordinarily helpful as the WIYN queue observers. We thank Gary Bernstein and Tony Tyson for developing and supporting the Big Throughput Camera at the CTIO 4-meter; this wide-field camera was important in the discovery of many of the high-redshift supernovae. David Schlegel, Doug Finkbeiner, and Marc Davis provided early access to, and helpful discussions concerning, their models of Galactic extinction. Megan Donahue contributed serendipitous HST observations of SN 1996cl. We thank Daniel Holz and Peter Höflich for helpful discussions. The larger computations described in this paper were performed at the U. S. Department of Energy's National Energy Research Science Computing Center (NERSC). This work was supported in part by the Physics Division, E. O. Lawrence Berkeley National Laboratory of the U. S. Department of Energy under Contract No. DE-AC03-76SF000098, and by the National Science Foundation's Center for Particle Astrophysics, University of California, Berkeley under grant No. ADT-88909616. A. V. F. acknowledges the support of NSF grant No. AST-9417213 and A. G. acknowledges the support of the Swedish Natural Science Research Council. The France-Berkeley Fund and the Stockholm-Berkeley Fund provided additional collaboration support.

APPENDIX

EXTINCTION CORRECTION USING A BAYESIAN PRIOR

Bayes Theorem provides a means of estimating the *a posteriori* probability distribution, $P(A|A_m)$, of a variable A given a measurement of its value, A_m, along with *a priori* information, $P(A)$, about what values are likely:

$$P(A|A_m) = \frac{P(A_m|A)P(A)}{\int P(A_m|A)P(A)dA} \tag{A1}$$

In practice $P(A)$ often is not well known, but must be estimated from sketchy, and possibly biased, data. For our purposes here we wish to distinguish between the true probability distribution, $P(A)$, and its estimated or assumed distribution, often called the Bayesian prior, which we denote as $\mathcal{P}(A)$. Riess, Press, & Kirshner (1996; RPK) present a Bayesian method of correcting SNe Ia for host galaxy extinction. For $\mathcal{P}(A)$ they assume a one-sided Gaussian function of extinction, $\mathcal{G}(A)$, with dispersion $\sigma_\mathcal{G} = 1$ magnitude:

$$\mathcal{P}(A) = \mathcal{G}(A) \equiv \begin{cases} \sqrt{\dfrac{2}{\pi\sigma_\mathcal{G}^2}}\, e^{-A^2/2\sigma_\mathcal{G}^2} & \text{for } A \geq 0 \\ 0 & \text{for } A < 0 \end{cases} \tag{A2}$$

which reflects the fact that dust can only redden and dim the light from a supernova. The probability distribution of the measured extinction, A_m, is an ordinary Gaussian with dispersion σ_m, i.e., the measurement uncertainty. RPK choose the most probable value of $P(A|A_m)$ as their best estimate of the extinction for each supernova:

$$\hat{A}_{\mathcal{G}} = \text{mode}(P(A|A_m)) = \begin{cases} \dfrac{A_m \sigma_{\mathcal{G}}^2}{\sigma_{\mathcal{G}}^2 + \sigma_m^2} & \text{for } A_m > 0 \\ 0 & \text{for } A_m \leq 0 \end{cases} \tag{A3}$$

Although this method provides the best estimate of the extinction correction for an individual supernova provided $\mathcal{P}(A) = P(A)$, once measurement uncertainties are considered its application to an ensemble of SNe Ia can result in a biased estimate of the ensemble average extinction whether or not $\mathcal{P}(A) = P(A)$. An extreme case which illustrates this point is where the true extinction is zero for all supernovae, i.e., P(A) is a delta function at zero. In this case, a measured value of $E(B{-}V) < 0$ (too blue) results in an extinction estimate of $\hat{A}_{\mathcal{G}} = 0$, while a measured value with $E(B{-}V) \geq 0$ results in an extinction estimate $\hat{A}_{\mathcal{G}} > 0$. The ensemble mean of these extinction estimates will be

$$\langle \hat{A}_{\mathcal{G}} \rangle = \frac{\sigma_m}{\sqrt{2\pi}} \left(\frac{\sigma_{\mathcal{G}}^2}{\sigma_{\mathcal{G}}^2 + \sigma_m^2} \right), \tag{A4}$$

rather than 0 as it should be. (This result is changed only slightly if the smaller uncertainties assigned to the least extincted SNe Ia are incorporated into a weighted average.)

The amount of this bias is dependent on the size of the extinction-measurement uncertainties, $\sigma_m = \mathcal{R}_B \sigma_{E(B-V)}$. For our sample of high-redshift supernovae, typical values of this uncertainty are $\sigma_m \sim 0.5$, while for the low-redshift supernovae, $\sigma_m \sim 0.07$. Thus, if the true extinction distribution is a delta-function at $A = 0$, while the one-sided prior, $\mathcal{G}(A)$, of Equation A2 is used, the bias in $\langle \hat{A}_{\mathcal{G}} \rangle$ is about 0.13 mag in the sense that the high-redshift supernovae would be overcorrected for extinction. Clearly, the exact amount of bias depends on the details of the dataset (e.g., color uncertainty, relative weighting). the true distribution $P(A)$, and the choice of prior $\mathcal{P}(A)$. This is a worst-case estimate, since we believe that the true extinction distribution is more likely to have some tail of events with extinction. Indeed, numerical calculations using a one-sided Gaussian for the true distribution, $P(A)$, show that the amount of bias decreases as the Gaussian width increases away from a delta function, crosses zero when $P(A)$ is still *much narrower* than $\mathcal{P}(A)$, and then increases with opposite sign. One might use the mean of $P(A|A_m)$ instead of the mode in equation A-3, since the bias then vanishes if $\mathcal{P}(A) = P(A)$, however this mean-calculated bias is even more sensitive to $\mathcal{P}(A) \neq P(A)$ than the mode-calculated bias.

We have only used conservative priors (which are somewhat broader than the true distribution, as discussed in Section 4.1), however it is instructive to consider the bias that results for a less conservative choice of prior. For example, an extinction distribution with only half of the supernovae distributed in a one-sided Gaussian and half in a delta function at zero extinction is closer to the simulations given by Hatano, Branch, & Deaton (1997). The presence of the delta-function component in this less conservative prior assigns zero extinction to the vast majority of supernovae, and thus cannot produce a bias even with different uncertainties at low and high redshift. This will lower the overall bias, but it will also assign zero extinction to many more supernovae than assumed in the prior, in typical cases in which the measurement uncertainty is not significantly smaller than the true extinction distribution. A restrictive prior, i.e. one which is actually narrower than the true distribution, can even lead to a bias in the opposite direction from a conservative prior.

It is clear from Bayes Theorem itself that the correct procedure for determining the maximum-likelihood extinction, $\tilde{A}$, of an ensemble of supernovae is to first calculate the *a posteriori* probability distribution for the ensemble:

$$P(A|\{A_{m_i}\}) = \frac{P(A) \sum P(A_{m_i}|A)}{\int P(A) \sum P(A_{m_i}|A) dA} \tag{A5}$$

and then take the most probable value of $P(A|\{A_{m_i}\})$ for $\tilde{A}$. For the above example of no reddening, this returns the correct value of $\tilde{A} = 0$.

In fitting the cosmological parameters generally one is not quite as interested in the ensemble extinction as in the combined impact of individual extinctions. In this case $P(A|\{A_{m_i}\})$ must be combined with other sources of uncertainty for each supernova in a maximum–likelihood fit, or the use of a Bayesian prior must be abandoned. In the former case a χ^2 fit is no longer appropriate since the individual $P(A|\{A_{m_i}\})$'s are strongly non-Gaussian. Use of a Gaussian uncertainty for $\hat{A}_{\mathcal{G}}$ based on the second–moment of $P(A|\{A_{m_i}\})$ may introduce additional biases.

References

Baade 1938, ApJ, 88, 285

Bahcall, N. A., & Fan, X. 1998, Ap.J. (also available at astro-ph/9803277), in press

Bernstein, G., & Tyson, J. A. 1998, http://www.astro.lsa.umich.edu/btc/user.html

Branch, D. 1998, Ann. Rev. Astro. Astrophys., 36, 17

Branch, D., Lacy, C. H., McCall, M. L., Sutherland, P. G., Uomoto, A., Wheeler, J. C., & Wills, B. J. 1983, ApJ, 270, 123

Burstein, D., & Heiles, C. 1982, AJ, 87, 1165

Burstein, D., & Heiles, C. 1998, private communication

Caldwell, R. R., Dave, R., & Steinhardt, P. J. 1998, Phys. Rev. Lett., 80, 1582

Cappellaro, E., Turatto, M., & Fernley, J. 1995. IUE - ULDA Access Guide No. 6: Supernovae, The Netherlands: ESA

Cardelli, J. A., Clayton, G. C., & Mathis, J. S. 1989, ApJ, 345, 245

Carlberg, R. G. 1997, astro-ph/9708054

Carlberg, R. G., et al. 1998, astro-ph/9804312

Carlberg, R. G., Yee, H. K. C., Ellingson, E., Abraham, R., Gravel, P., Morris, S., & Pritchet, C. J. 1996, ApJ, 462, 32

Carroll, S. M., Press, W. H., & Turner, E. L. 1992, Ann. Rev. Astro. Astrophys., 30, 499

Chaboyer, B., DeMarque, P., Kernan, P. J., & Krauss, L. M. 1998, ApJ, 494, 96

Chiba, M., & Yoshii, Y. 1998, astro-ph/9808321

Clayton, G. C., & Cardelli, J. A. 1988, AJ, 96, 695

Colgate, S. 1979, ApJ, 232, 404

Daly, R. A., Guerra, E. J., & Wan, L. 1998, astro-ph/9803265

Efstathiou, G., et al. 1998, in preparation

Falco, E. E., Kochanek, C. S., & Munoz, J. A. 1998, ApJ, 494, 47

Feldman, G. J., & Cousins, R. D. 1998, Phys. Rev. D, 57, 3873

Filippenko, A. V., et al. 1998, in preparation

Freedman, W. L., Mould, J. R., Kennicut, R. C., & Madore, B. F. 1998. In IAU Symposium 183, pages (astro–ph/9801080)

Frieman, J. A. 1996, astro-ph/9608068

Fukugita, M., Hogan, C. J., & Peebles, P. J. E. 1997, astro-ph/9712020

Garnavich, P., et al. 1998a, ApJ, 493, L53

Garnavich, P., et al. 1998b, ApJ, 509, in press

Goldhaber, G., et al. 1995. In Presentations at the NATO ASI in Aiguablava, Spain, LBL-38400, page III.1; also published in Thermonuclear Supernova, P. Ruiz-Lapuente, R. Canal, and J.Isern, editors, Dordrecht: Kluwer, page 777 (1997)

Goldhaber, G., et al. 1998, Ap.J., in preparation

Goobar, A., & Perlmutter, S. 1995, ApJ, 450, 14

Gordon, K. D., & Clayton, G. C. 1998, ApJ, 500, 816

Gratton, R. G., Pecci, F. F., Carretta, E., Clementina, G., Corsi, C. E., & Lattanzi, M. 1997, ApJ, 491, 749

Guerra, E. J., & Daly, R. A. 1998, ApJ, 493, 536

Hamuy, M., Phillips, M. M., Maza, J., Suntzeff, N. B., Schommer, R. A., & Aviles, R. 1995, AJ, 109, 1

Hamuy, M., Phillips, M. M., Maza, J., Suntzeff, N. B., Schommer, R. A., & Aviles, R. 1996, AJ, 112, 2391

Hatano, K., Branch, D., & Deaton, J. 1997, astro-ph/9711311

Höflich, P., & Khokhlov, A. 1996, ApJ, 457, 500

Höflich, P., Wheeler, J. C., & Thielemann, F. K. 1998, ApJ, 495, 617

Holz, D. E., & Wald, R. M. 1998, Phys. Rev. D, 58, 063501

Hook, I. M., Nugent, P., et al. 1998, in preparation

Jeffery, D., Leibundgut, B., Kirshner, R. P., Benetti, S., Branch, D., & Sonneborn, G. 1992, ApJ, 397, 304

Kantowski, R. 1998, ApJ, 88, 285.

Kayser, R., Helbig, P., & Schramm T. 1996, A&A, 318, 680.

Kim, A., et al. 1998, ApJ, in preparation

Kim, A., Goobar, A., & Perlmutter, S. 1996, PASP, 108, 190

Kirshner, R., et al. 1993, ApJ, 415, 589

Kirshner, R., & Oke, J. 1975, ApJ, 200, 574

Kochanek, C. S. 1996, ApJ, 466, 638

Leibundgut, B., et al. 1996a, Ap.J.Lett., 466, L21

Leibundgut B. et al. 1996b, Ap.J.Lett., 371, L23

Lineweaver, C. H. 1998, ApJ, Lett., in press

Maddox, S. J., Sutherland, W. J., Loveday, J., & Peterson, B. A. 1990, MNRAS, 247, 1P

Malmquist, K. G. 1924, Medd. Lund Astron. Obs. Ser. II, No. 32, 64

Malmquist, K. G. 1936, Stockholm Obs. Medd., No. 26

Marvin, H., & Perlmutter, S., 1989, IAU Circ. No. 4727

Meikle, W. P. S., et al. 1996, MNRAS, 281, 263

Mihalas, D., & Binney, J. 1981. Galactic Astronomy: Structure and Kinematics, 2nd ed., San Francisco: W.H. Freeman

Nørgaard-Nielsen, et al. 1989, Nature, 339, 523

Nugent, P., Branch, D., Baron, E., Fisher, A., Vaughan, T., & Hauschildt, P. 1995, Phys.Rev.Lett., 75, 394, and erratum, 75, 1874

Nugent, P., et al. 1998, PASP, in preparation

Oke, J., et al. 1995, PASP, 107, 375

Oliver, S. J., Rowan-Robinson, M., Broadhurst, T. J., McMahon, R. G., Saunders, W., Taylor, A., Lawrence, A., Lonsdale, C. J., Hacking, P., & Conrow, T. 1996, MNRAS, 280, 673

Pain, R., et al. 1996, ApJ, 473, 356

Patat, F., et al. 1996, MNRAS, 278, 111

Pei, Y. C. 1992, ApJ, 395, 130

Perlmutter, S., et al. 1995a. In Presentations at the NATO ASI in Aiguablava, Spain, LBL-38400, page I.1; also published in Thermonuclear Supernova, P. Ruiz-Lapuente, R. Canal, and J.Isern, editors, Dordrecht: Kluwer, page 749 (1997)

Perlmutter, S., et al. 1995b, IAU Circ. No. 6270

Perlmutter, S., et al. 1996, IAU Circ. No. 6621

Perlmutter, S., et al. 1997a, IAU Circ. No. 6596

Perlmutter, S., et al. 1997b, IAU Circ. No. 6540

Perlmutter, S., et al. 1997c, IAU Circ. No. 6646

Perlmutter, S., et al. 1997d, IAU Circ. No. 6804

Perlmutter, S., et al. 1997e, ApJ, 483, 565 [P97]

Perlmutter, S., et al. 1998a, IAU Circ. No. 6881

Perlmutter, S., et al. 1998b, Nature, 391, 51 and erratum (on author list), 392, 311

Perlmutter, S., et al. 1998c. In Presentation at the January 1998 Meeting of the American Astronomical Society, Washington, D.C., LBL-42230, available at www-supernova.lbl.gov and astro-ph; referenced in B.A.A.S., volume 29, page 1351 (1997)

Pettini, M., King, D. L., Smith, L. J., & Hunstead, R. W. 1997, ApJ, 478, 536

Phillips, M., et al. 1998, ApJ, in preparation

Phillips, M. M. 1993, Ap.J.Lett., 413, L105

Phillips, M. M. 1998, private communication

Phillips, M. M., et al. 1987, PASP, 99, 592

Riess, A., et al. 1997a, AJ, 114, 722

Riess, A., Davis, M., Baker, J., & Kirshner, R. P. 1997b, ApJ, 488, L1

Riess, A. G., et al. 1998, AJ, 116, 1009 (in press)

Riess, A. G., Press, W. H., & Kirshner, R. P. 1995, ApJ, 438, L17

Riess, A. G., Press, W. H., & Kirshner, R. P. 1996, ApJ, 473, 88

Ruiz-Lapuente, P. 1998. In Proceedings of the Second Heidelberg Conference on Dark Matter in Astro and Particle Physics, Klapdor-Kleingrothaus *et al.*, editors, to be published

Ruiz-Lapuente, P., Canal, R., & Burkert, A. 1997. In Thermonuclear Supernova, P. Ruiz-Lapuente, R. Canal, and J.Isern, editors, Dordrecht: Kluwer, page 205

Saha, A., et al. 1997, ApJ, 486, 1

Schlegel, D., Finkbeiner, D., & Davis, M. 1998, ApJ, in press

Schmidt, B. P., et al. 1998, ApJ, in press

Schramm, D. N. 1990. In Astrophysical Ages and Dating Methods, E. Vangioni-Flam *et al.*, editors, Gif sur Yvette: Edition Frontiers, page 365

Sigad, Y., Eldar, A., Dekel, A., Strauss, M. A., & Yahil, A. 1998, ApJ, 495, 516

Smail, I., Hogg, D. W., Yan, L., & Cohen, J. G. 1995, ApJ, 449, L106

Steinhardt, P. J. 1996, Nature, 382, 768

Tammann, G. A. 1979. In ESA/ESO Workshop on Astronomical Uses of the Space Telescope, F. Macchetto, F. Pacini, and M. Tarenghi, editors, Geneva: ESO, page 329

Tegmark, et al. 1998, astro-ph/9805117

Tripp, R. 1998, A&A, 331, 815

Turner, M. S., & White, M. 1997, Phys. Rev. D, 56, R4439

Vacca, W. D., & Leibundgut, B. 1996, ApJ, 471, L37

Wambsganss, J., Cen, R., & Ostriker, J. P. 1998, ApJ, 494, 29

Wang, L., Höflich, P., & Wheeler, J. C. 1997, ApJ, 483, L29

White, M. 1998, astro-ph/9802295

Willick, J. A. 1994, ApJS, 92, 1

Willick, J. A., & Strauss, M. A. 1998, ApJ, 507, 64

Willick, J. A., Strauss, M. A., Dekel, A., & Tsafrir, K. 1997, ApJ, 486, 629

Zlatev, I., Wang, L., & Steinhardt, P. J. 1998, astro-ph/9807002

TABLE 1
SCP SNE IA DATA

SN (1)	z (2)	σ_z (3)	$m_X^{\rm peak}$ (4)	$\sigma_X^{\rm peak}$ (5)	A_X (6)	K_{BX} (7)	$m_B^{\rm peak}$ (8)	$m_B^{\rm effective}$ (9)	$\sigma_{m_B^{\rm effective}}$ (10)	Notes (11)
1992bi	0.458	0.001	22.12	0.10	0.03	−0.72	22.81	23.11	0.46	E–H
1994F	0.354	0.001	22.08	0.10	0.11	−0.58	22.55	22.38	0.33	E–H
1994G	0.425	0.001	21.52	0.21	0.03	−0.68	22.17	22.13	0.49	
1994H	0.374	0.001	21.28	0.06	0.10	−0.61	21.79	21.72	0.22	B–L
1994al	0.420	0.001	22.37	0.06	0.42	−0.68	22.63	22.55	0.25	E–H
1994am	0.372	0.001	21.82	0.07	0.10	−0.61	22.32	22.26	0.20	E–H
1994an	0.378	0.001	22.14	0.08	0.21	−0.62	22.55	22.58	0.37	E–H
1995aq	0.453	0.001	22.60	0.07	0.07	−0.71	23.24	23.17	0.25	
1995ar	0.465	0.005	22.71	0.04	0.07	−0.71	23.35	23.33	0.30	H
1995as	0.498	0.001	23.02	0.07	0.07	−0.71	23.66	23.71	0.25	H
1995at	0.655	0.001	22.62	0.03	0.07	−0.66	23.21	23.27	0.21	H
1995aw	0.400	0.030	21.75	0.03	0.12	−0.65	22.27	22.36	0.19	
1995ax	0.615	0.001	22.53	0.07	0.11	−0.67	23.10	23.19	0.25	
1995ay	0.480	0.001	22.64	0.04	0.35	−0.72	23.00	22.96	0.24	
1995az	0.450	0.001	22.44	0.07	0.61	−0.71	22.53	22.51	0.23	
1995ba	0.388	0.001	22.08	0.04	0.06	−0.63	22.66	22.65	0.20	
1996cf	0.570	0.010	22.70	0.03	0.13	−0.68	23.25	23.27	0.22	
1996cg	0.490	0.010	22.46	0.03	0.11	−0.72	23.06	23.10	0.20	C,D,G–L
1996ci	0.495	0.001	22.19	0.03	0.09	−0.71	22.82	22.83	0.19	
1996ck	0.656	0.001	23.08	0.07	0.13	−0.66	23.62	23.57	0.28	
1996cl	0.828	0.001	23.53	0.10	0.18	−1.22	24.58	24.65	0.54	
1996cm	0.450	0.010	22.66	0.07	0.15	−0.71	23.22	23.17	0.23	
1996cn	0.430	0.010	22.58	0.03	0.08	−0.69	23.19	23.13	0.22	C,D,G–L
1997F	0.580	0.001	22.90	0.06	0.13	−0.68	23.45	23.46	0.23	H
1997G	0.763	0.001	23.56	0.41	0.20	−1.13	24.49	24.47	0.53	
1997H	0.526	0.001	22.68	0.05	0.16	−0.70	23.21	23.15	0.20	H
1997I	0.172	0.001	20.04	0.02	0.16	−0.33	20.20	20.17	0.18	
1997J	0.619	0.001	23.25	0.08	0.13	−0.67	23.80	23.80	0.28	
1997K	0.592	0.001	23.73	0.10	0.07	−0.67	24.33	24.42	0.37	H
1997L	0.550	0.010	22.93	0.05	0.08	−0.69	23.53	23.51	0.25	
1997N	0.180	0.001	20.19	0.01	0.10	−0.34	20.42	20.43	0.17	H
1997O	0.374	0.001	22.97	0.07	0.09	−0.61	23.50	23.52	0.24	B–L
1997P	0.472	0.001	22.52	0.04	0.10	−0.72	23.14	23.11	0.19	
1997Q	0.430	0.010	22.01	0.03	0.09	−0.69	22.60	22.57	0.18	
1997R	0.657	0.001	23.28	0.05	0.11	−0.66	23.83	23.83	0.23	
1997S	0.612	0.001	23.03	0.05	0.11	−0.67	23.59	23.69	0.21	
1997ac	0.320	0.010	21.38	0.03	0.09	−0.55	21.83	21.86	0.18	
1997af	0.579	0.001	22.96	0.07	0.09	−0.68	23.54	23.48	0.22	
1997ai	0.450	0.010	22.25	0.05	0.14	−0.71	22.81	22.83	0.30	H
1997aj	0.581	0.001	22.55	0.06	0.11	−0.68	23.12	23.09	0.22	
1997am	0.416	0.001	21.97	0.03	0.11	−0.67	22.52	22.57	0.20	
1997ap	0.830	0.010	23.20	0.07	0.13	−1.23	24.30	24.32	0.22	H

Col 1. IAU Name assigned to SCP supernova.
Col 2. Geocentric redshift of supernova or host galaxy.
Col 3. Redshift uncertainty.
Col 4. Peak magnitude from lightcurve fit in observed band corresponding to restframe B-band (i.e. $m_X^{\rm peak} \equiv m_R^{\rm peak}$ or $m_I^{\rm peak}$).
Col 5. Uncertainty in fit peak magnitude.
Col 6. Galactic extinction in observed band corresponding to restframe B-band (i.e., $A_X \equiv A_R$ or A_I); an uncertainty of 10% is assumed.
Col 7. Representative K-correction (at peak) from observed band to B-band (i.e., $K_{BX} \equiv K_{BR}$ or K_{BI}); an uncertainty of 2% is assumed.
Col 8. B-band peak magnitude.
Col 9. Stretch-luminosity corrected effective B-band peak magnitude: $m_B^{\rm effective} \equiv m_X^{\rm peak} + \alpha(s-1) - K_{BX} - A_X$.
Col 10. Total uncertainty in corrected B-band peak magnitude. This includes uncertainties due to the intrinsic luminosity dispersion of SNe Ia of 0.17 mag, 10% of the Galactic extinction correction, 0.01 mag for K-corrections, 300 km s^{-1} to account for peculiar velocities, in addition to propagated uncertainties from the lightcurve fits.
Col 11. Fits from which given supernova was excluded.

TABLE 2
CALÁN TOLOLO SNE IA DATA

SN (1)	z (2)	σ_z (3)	$m_{obs}^{\rm peak}$ (4)	$\sigma_{obs}^{\rm peak}$ (5)	A_B (6)	K_{BB} (7)	$m_B^{\rm peak}$ (8)	$m_B^{\rm corr}$ (9)	$\sigma_{m_B^{\rm corr}}$ (10)	Notes (11)
1990O	0.030	0.002	16.62	0.03	0.39	–0.00	16.23	16.26	0.20	
1990af	0.050	0.002	17.92	0.01	0.16	+0.01	17.75	17.63	0.18	
1992P	0.026	0.002	16.13	0.03	0.12	–0.01	16.02	16.08	0.24	
1992ae	0.075	0.002	18.61	0.12	0.15	+0.03	18.43	18.43	0.20	
1992ag	0.026	0.002	16.59	0.04	0.38	–0.01	16.22	16.28	0.20	
1992al	0.014	0.002	14.60	0.01	0.13	–0.01	14.48	14.47	0.23	
1992aq	0.101	0.002	19.29	0.12	0.05	+0.05	19.19	19.16	0.23	
1992bc	0.020	0.002	15.20	0.01	0.07	–0.01	15.13	15.18	0.20	
1992bg	0.036	0.002	17.41	0.07	0.77	+0.00	16.63	16.66	0.21	
1992bh	0.045	0.002	17.67	0.04	0.10	+0.01	17.56	17.61	0.19	
1992bl	0.043	0.002	17.31	0.07	0.04	+0.01	17.26	17.19	0.18	
1992bo	0.018	0.002	15.85	0.02	0.11	–0.01	15.75	15.61	0.21	B–L
1992bp	0.079	0.002	18.55	0.02	0.21	+0.04	18.30	18.27	0.18	
1992br	0.088	0.002	19.71	0.07	0.12	+0.04	19.54	19.28	0.18	B–L
1992bs	0.063	0.002	18.36	0.05	0.09	+0.03	18.24	18.24	0.18	
1993B	0.071	0.002	18.68	0.08	0.31	+0.03	18.34	18.33	0.20	
1993O	0.052	0.002	17.83	0.01	0.25	+0.01	17.58	17.54	0.18	
1993ag	0.050	0.002	18.29	0.02	0.56	+0.01	17.71	17.69	0.20	

Col 1. IAU Name assigned to Calán Tololo supernova.
Col 2. Redshift of supernova or host galaxy in Local Group restframe.
Col 3. Redshift uncertainty.
Col 4. Peak magnitude from lightcurve fit, in observed *B*-band. Note that the template lightcurve used in the fit is not identical to the template lightcurve used by Hamuy et al. so the best-fit peak magnitude may differ slightly.
Col 5. Uncertainty in fit peak magnitude.
Col 6. Galactic extinction in observed *B*-band; an uncertainty of 10% is assumed.
Col 7. Representative *K*-correction from observed *B*-band to restframe *B*-band; an uncertainty of 2% is assumed.
Col 8. *B*-band peak magnitude.
Col 9. Stretch–luminosity corrected *B*-band peak magnitude.
Col 10. Total uncertainty in corrected *B*-band peak magnitude. This includes uncertainties due to the intrinsic luminosity dispersion of SNe Ia of 0.17 mag, 10% of the Galactic extinction correction, 0.01 mag for *K*–corrections, 300 km s^{-1} to account for peculiar velocities, in addition to propagated uncertainties from the lightcurve fits.
Col 11. Fits from which given supernova was excluded.

TABLE 3
FIT RESULTS

Fit	N	χ^2	DOF	Ω_M^{flat}	$P(\Omega_\Lambda > 0)$	Best Fit Ω_M, Ω_Λ	Fit Description
Inclusive Fits							
A	60	98	56	$0.29^{+0.09}_{-0.08}$	0.9984	0.83,1.42	All SNe
B	56	60	52	$0.26^{+0.09}_{-0.08}$	0.9992	0.85,1.54	Fit A, but excluding 2 residual outliers and 2 stretch outliers
Primary Fit							
C	**54**	**56**	**50**	$\mathbf{0.28^{+0.09}_{-0.08}}$	**0.9979**	**0.73,1.32**	**Fit B, but also excluding 2 likely reddened**
Comparison Analysis Techniques							
D	54	53	51	$0.25^{+0.10}_{-0.09}$	0.9972	0.76,1.48	No stretch correction[a]
E	53	62	49	$0.29^{+0.12}_{-0.10}$	0.9894	0.35,0.76	Bayesian one-sided extinction corrected[b]
Effect of Reddest SNe							
F	51	59	47	$0.26^{+0.09}_{-0.08}$	0.9991	0.85,1.54	Fit B SNe with colors measured
G	49	56	45	$0.28^{+0.09}_{-0.08}$	0.9974	0.73,1.32	Fit C SNe with colors measured
H	40	33	36	$0.31^{+0.11}_{-0.09}$	0.9857	0.16,0.50	Fit G, but excluding 7 next reddest and 2 next faintest high-redshift SNe
Systematic Uncertainty Limits							
I	54	56	50	$0.24^{+0.09}_{-0.08}$	0.9994	0.80,1.52	Fit C with +0.03 mag systematic offset
J	54	57	50	$0.33^{+0.10}_{-0.09}$	0.9912	0.72,1.20	Fit C with –0.04 mag systematic offset
Clumped Matter Metrics							
K	54	57	50	$0.35^{+0.12}_{-0.10}$	0.9984	2.90,2.64	Empty beam metric[c]
L	54	56	50	$0.34^{+0.10}_{-0.09}$	0.9974	0.94,1.46	Partially filled beam metric

[a]0.24 mag intrinsic SNe Ia luminosity dispersion assumed.

[b]Bayesian method of Riess et al. (1996) with conservative prior (see text and Appendix A) and 0.10 mag intrinsic SNe Ia luminosity dispersion.

[c]Assumes additional Bayesian prior of $\Omega_M < 3, \Omega_\Lambda < 3$.

TABLE 4
SUMMARY OF UNCERTAINTIES AND CROSS-CHECKS

	Uncertainty[a] on $(\Omega_M^{flat}, \Omega_\Lambda^{flat}) = (0.28, 0.72)$	
(A) Calculated Identified Uncertainties		
Statistical Uncertainties (see §5)	$\sigma_{\Omega^{flat}_{M,\Lambda}} =$	
High-redshift SNe	0.05	
Low-redshift SNe	0.065	
Total	**0.085**	
Systematic Uncertainties from Identified Entities/Processes		
Dust that reddens (see §4.1.2) i.e., $\mathcal{R}_B(z=0.5) < 2\mathcal{R}_B(z=0)$	<0.03	
Malmquist bias difference (see §4.2)	<0.04	
K-correction uncertainty (see §2, §3) including zero-points	<0.025	
Evolution of average (see §4.4) SN Ia progenitor metallicity affecting rest-frame B spectral features	<0.01	
Total	**0.05**	
(B) Uncertainties Not Calculated		
Proposed/Theoretical Sources of Systematic Uncertainties		*Bounds and Tests (see text)*
Evolving grey dust (see §4.4, §4.1.3) i.e., $\mathcal{R}_B(z=0.5) > 2\mathcal{R}_B(z=0)$		Test with $\geq$3-filter color measurements.
Clumpy grey dust (see §5)		Would increase SN mag residual dispersion with z.
SN Ia evolution effects (see §4.4)[b] Shifting distribution of progenitor mass, metallicity, C/O ratio		Test that spectra match on appropriate date for all z. Compare low- and high-redshift lightcurve rise-times, and lightcurve timescales before and after maximum. Test width-luminosity relation for low-redshift SNe across wide range of environments. Compare low- and high-redshift subsets from ellipticals/spirals, cores/outskirts, etc.
(C) Cross Checks		
Sensitivity to (see §4.5)	$\Delta_{\Omega^{flat}_{M,\Lambda}} =$	
Width-luminosity relation	<0.03	
Non-SN Ia contamination	<0.05	
Galactic extinction model	<0.04	
Gravitational lensing (see §4.3) by clumped mass	<0.06	

[a]For the redshift distribution of supernovae in this work, uncertainties in $\Omega^{flat}_{M,\Lambda}$ correspond approximately to a factor of 1.3 times uncertainties in the relative supernova magnitudes. For ease of comparisons, this table does not distinguish the small differences between the positive and negative error bars; see Table 3 for these.

[b]The comparison of low- and high-redshift lightcurve rise-times discussed in Section 4.4 theoretically limits evolutionary changes in the zero-point of the lightcurve width-luminosity relation to less than ~0.1 mag, i.e. $\Delta_{\Omega^{flat}_{M,\Lambda}} \lesssim 0.13$.

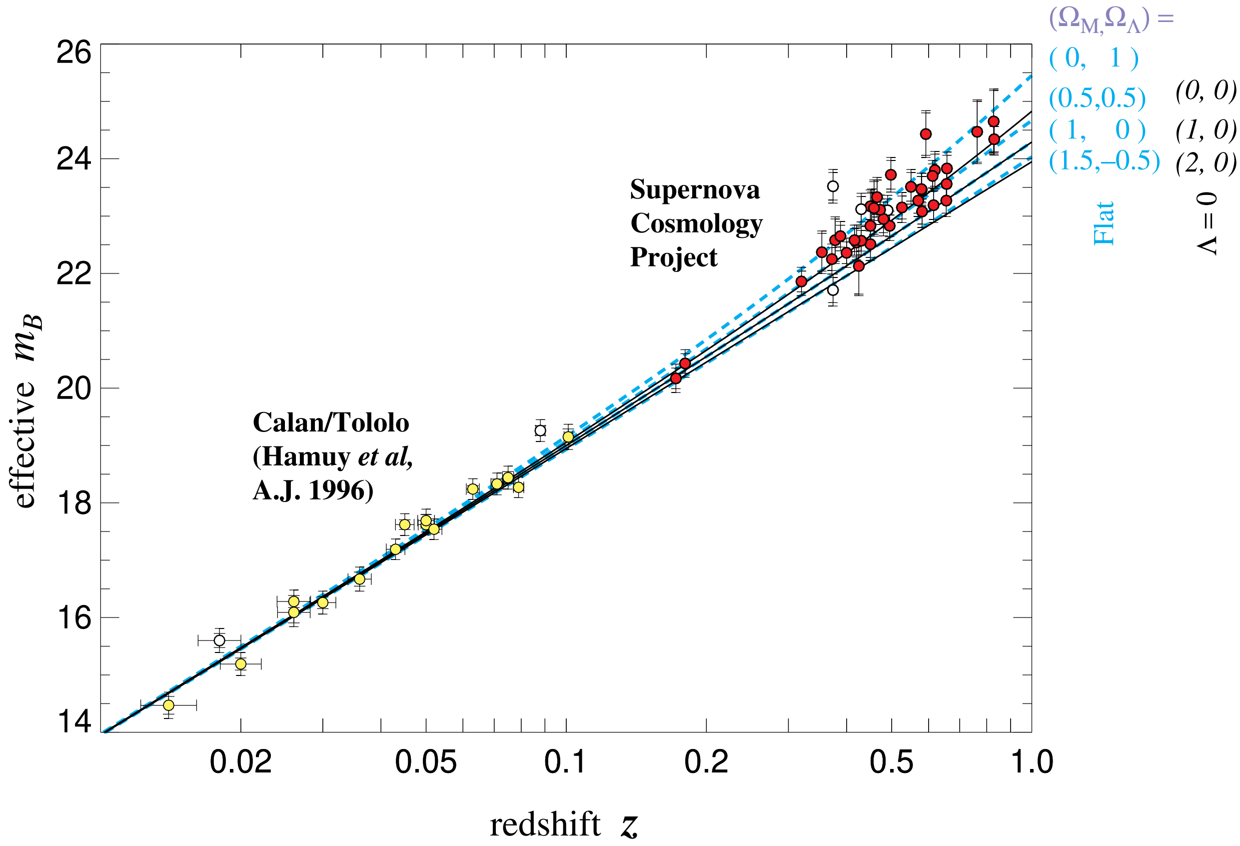

FIG. 1.— Hubble diagram for 42 high-redshift Type Ia supernovae from the Supernova Cosmology Project, and 18 low-redshift Type Ia supernovae from the Calán/Tololo Supernova Survey, after correcting both sets for the SN Ia lightcurve width-luminosity relation. The inner error bars show the uncertainty due to measurement errors, while the outer error bars show the total uncertainty when the intrinsic luminosity dispersion, 0.17 mag, of lightcurve-width-corrected Type Ia supernovae is added in quadrature. The unfilled circles indicate supernovae not included in Fit C. The horizontal error bars represent the assigned peculiar velocity uncertainty of 300 km s^{-1}. The solid curves are the theoretical $m_B^{\rm effective}(z)$ for a range of cosmological models with zero cosmological constant: $(\Omega_M, \Omega_\Lambda) = (0,0)$ on top, $(1,0)$ in middle and (2,0) on bottom. The dashed curves are for a range of flat cosmological models: $(\Omega_M, \Omega_\Lambda) = (0,1)$ on top, $(0.5,0.5)$ second from top, $(1,0)$ third from top, and (1.5,-0.5) on bottom.

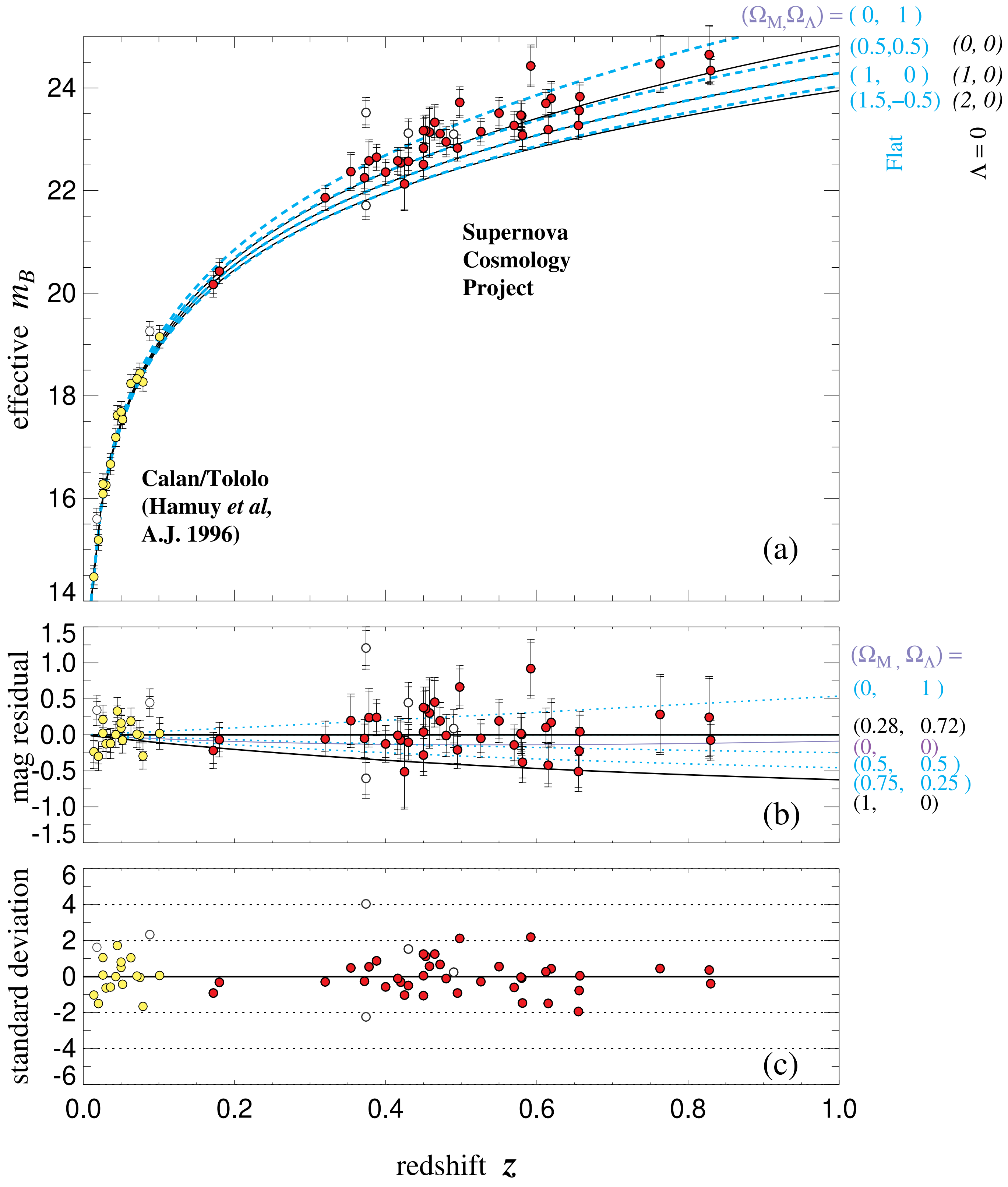

$(\Omega_M,\Omega_\Lambda) = (0, 1)$
(0.5,0.5)
(0, 0)
(1, 0)
(1, 0)
(1.5,–0.5)
(2, 0)
Flat
$\Lambda = 0$
effective m_B
Supernova Cosmology Project
Calan/Tololo (Hamuy et al, A.J. 1996)
(a)
mag residual
$(\Omega_M, \Omega_\Lambda) =$
(0, 1)
(0.28, 0.72)
(0, 0)
(0.5, 0.5)
(0.75, 0.25)
(1, 0)
(b)
standard deviation
(c)
redshift z

FIG. 2.—

(a) Hubble diagram for 42 high-redshift Type Ia supernovae from the Supernova Cosmology Project, and 18 low-redshift Type Ia supernovae from the Calán/Tololo Supernova Survey, plotted on a linear redshift scale to display details at high redshift. The symbols and curves are as in Figure 1. (b) The magnitude residuals from the best-fit flat cosmology for the Fit C supernova subset, $(\Omega_{\rm M},\Omega_\Lambda) = (0.28, 0.72)$. The dashed curves are for a range of flat cosmological models: $(\Omega_{\rm M},\Omega_\Lambda) = (0, 1)$ on top, $(0.5, 0.5)$ third from bottom, $(0.75, 0.25)$ second from bottom, and (1,0) is the solid curve on bottom. The middle solid curve is for $(\Omega_{\rm M},\Omega_\Lambda) = (0, 0)$. Note that this plot is practically identical to the magnitude residual plot for the best-fit unconstrained cosmology of Fit C, with $(\Omega_{\rm M},\Omega_\Lambda) = (0.73, 1.32)$. (c) The uncertainty-normalized residuals from the best-fit flat cosmology for the Fit C supernova subset, $(\Omega_{\rm M},\Omega_\Lambda) = (0.28, 0.72)$.

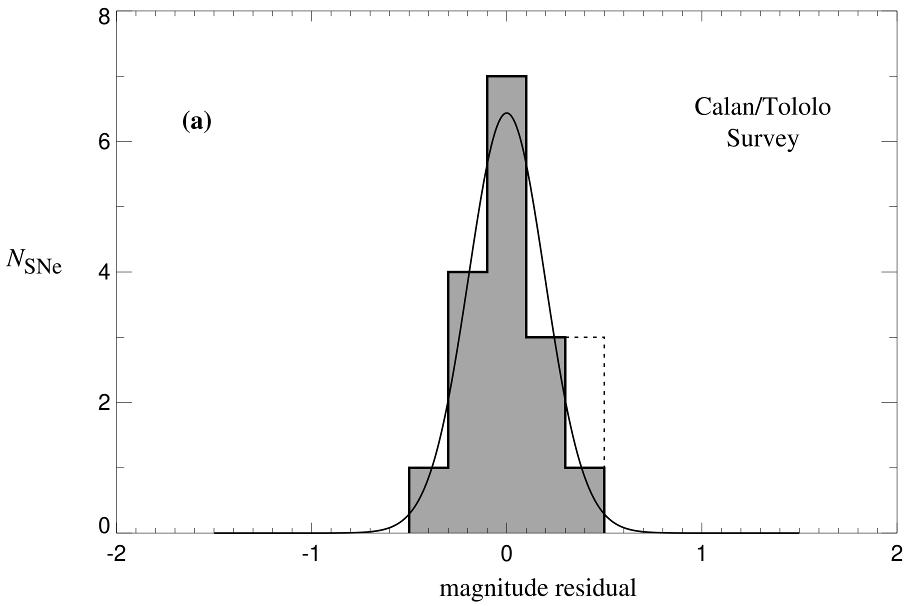

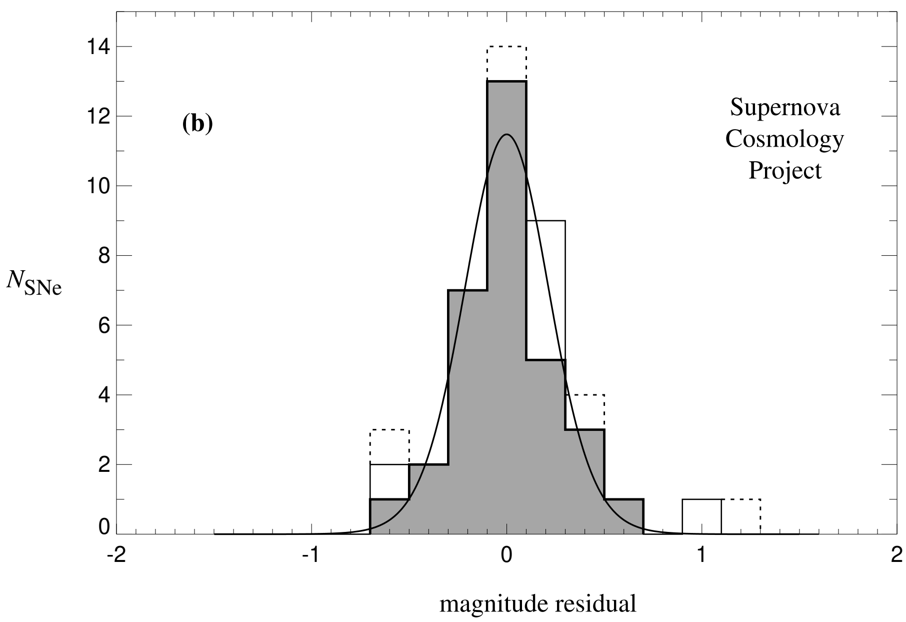

FIG. 3.— The distribution of restframe *B*-band magnitude residuals from the best-fit flat cosmology for the Fit C supernova subset, for (a) 18 Calán/Tololo supernovae, at redshifts $z \leq 0.1$ and (b) 42 supernovae from the Supernova Cosmology Project, at redshifts between 0.18 and 0.83. The darker shading indicates those residuals with uncertainties less than 0.35 mag, unshaded boxes indicate uncertainties greater than 0.35 mag, and dashed boxes indicate the supernovae that are excluded from Fit C. The curves show the expected magnitude residual distributions if they are drawn from normal distributions given the measurement uncertainties and 0.17 mag of intrinsic SN Ia dispersion. The low-redshift expected distribution matches a Gaussian with $\sigma = 0.20$ mag (with error on the mean of 0.05 mag), while the high-redshift expected distribution matches a Gaussian with $\sigma = 0.22$ mag (with error on the mean of 0.04 mag).

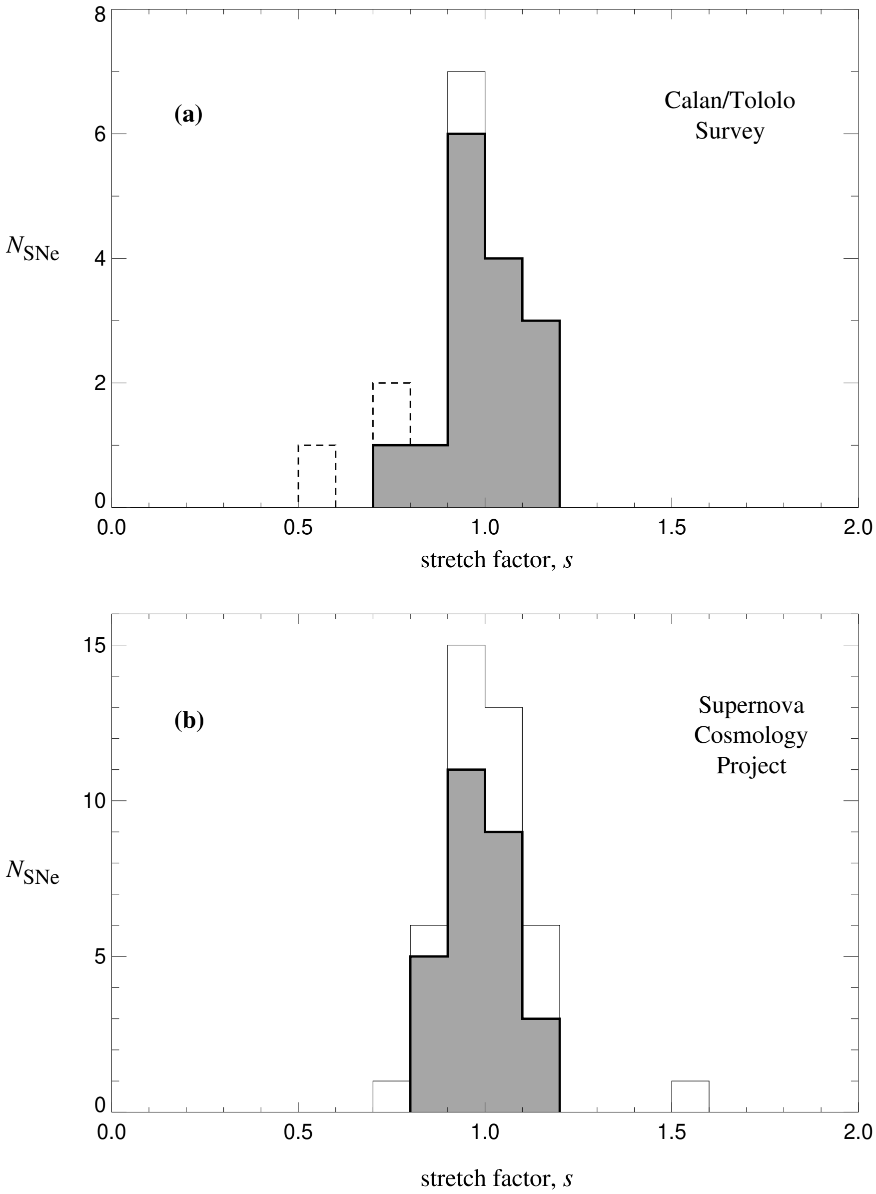

FIG. 4.— The distribution of lightcurve widths for (a) 18 Calán/Tololo supernovae, at redshifts $z \leq 0.1$ and (b) 42 supernovae from the Supernova Cosmology Project, at redshifts between 0.18 and 0.83. The lightcurve widths are characterized by the "stretch factor," s, that stretches or contracts the time axis of a template SN Ia lightcurve to best fit the observed lightcurve for each supernova (see Perlmutter et al. 1995a, 1997e; Kim et al. 1998; Goldhaber et al. 1998). The template has been time-dilated by a factor $1+z$ before fitting to the observed lightcurves to account for the cosmological lengthening of the supernova timescale (Goldhaber et al. 1995; Leibundgut et al. 1996a). The shading indicates those measurements of s with uncertainties less than 0.1, and the dashed lines indicate the two supernovae that are removed from the fits after Fit A. These two excluded supernovae are the most significant deviations from $s = 1$ (the highest-stretch supernova in panel (b) has an uncertainty of ± 0.23 and hence is not a significant outlier from $s = 1$); the remaining low- and high-redshift distributions have almost exactly the same error-weighted means: $\langle s \rangle_{\mathrm{Hamuy}} = 0.99 \pm 0.01$ and $\langle s \rangle_{\mathrm{SCP}} = 1.00 \pm 0.01$.

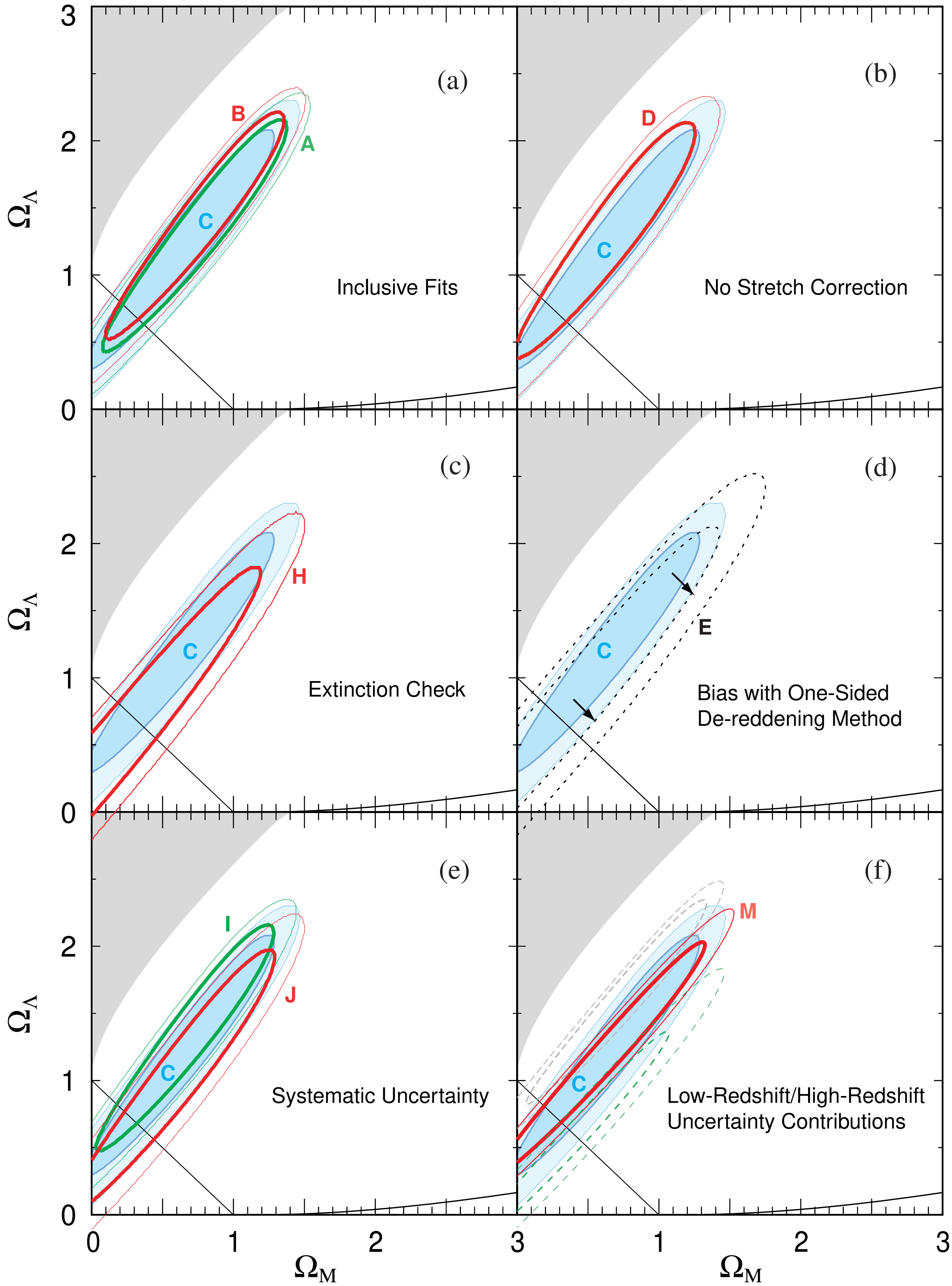
(a)
B
A
C
Inclusive Fits
(b)
D
C
No Stretch Correction
(c)
H
C
Extinction Check
(d)
E
C
Bias with One-Sided
De-reddening Method
(e)
I
J
C
Systematic Uncertainty
(f)
M
C
Low-Redshift/High-Redshift
Uncertainty Contributions
Ω_Λ
Ω_M
0
1
2
3

FIG. 5.—

Comparison of best-fit confidence regions in the Ω_M–Ω_Λ plane. Each subpanel shows the result of Fit C (shaded regions) compared with fits to different subsets of supernovae, or variant analyses for the same subset of supernovae, to test the robustness of the Fit C result. Unless otherwise indicated, the 68% and 90% confidence regions in the Ω_M–Ω_Λ plane are shown, after integrating the four-dimensional fits over the other two variables, $\mathcal{M}_B$ and α. The "no-big-bang" upper-left shaded region, the flat-universe diagonal line, and the infinite expansion line are shown as in Figure 7 for ease of comparison. The subpanels show: (a) Fit A of all 60 supernovae; and Fit B of 56 supernovae, excluding the two outliers from the lightcurve width distribution and the two remaining statistical outliers. Fit C further excludes the two likely reddened high-redshift supernovae. (b) Fit D of the same 54-supernova subset as in Fit C, but with no correction for the lightcurve width-luminosity relation. (c) Fit H of the subset of supernovae with color measurements, after excluding the reddest 25% (9 high-redshift supernovae) and the two faint high-redshift supernovae with large uncertainties in their color measurements. The close match to the confidence regions of Fit C indicates that any extinction of these supernovae is quite small, and not significant in the fits of the cosmological parameters. (d) The 68% confidence region for Fit E of the 53 supernovae with color measurements from the Fit B dataset, but following the Bayesian reddening-correction method of Riess, Press, & Kirshner (1996). This method, when used with any reasonably conservative prior (i.e., somewhat broader than the likely true extinction distribution; see text), can produce a result that is biased, with an approximate bias direction and worst-case amount indicated by the arrows. (e) Fits I and J are identical to Fit C, but with 0.03 or 0.04 magnitudes added or subtracted from each of the high-redshift supernova measurements, to account for the full range of identified systematic uncertainty in each direction. Other hypothetical sources of systematic uncertainty (see Table 4B) are not included. (f) Fit M is a separate two-parameter (Ω_M and Ω_Λ) fit of just the high-redshift supernovae, using the values of $\mathcal{M}_B$ and α found from the low redshift supernovae. The dashed confidence regions show the approximate range of uncertainty from these two low-redshift-derived parameters, added to the systematic errors of Fit J. Future well-observed low-redshift supernovae can constrain this dashed-line range of uncertainty.

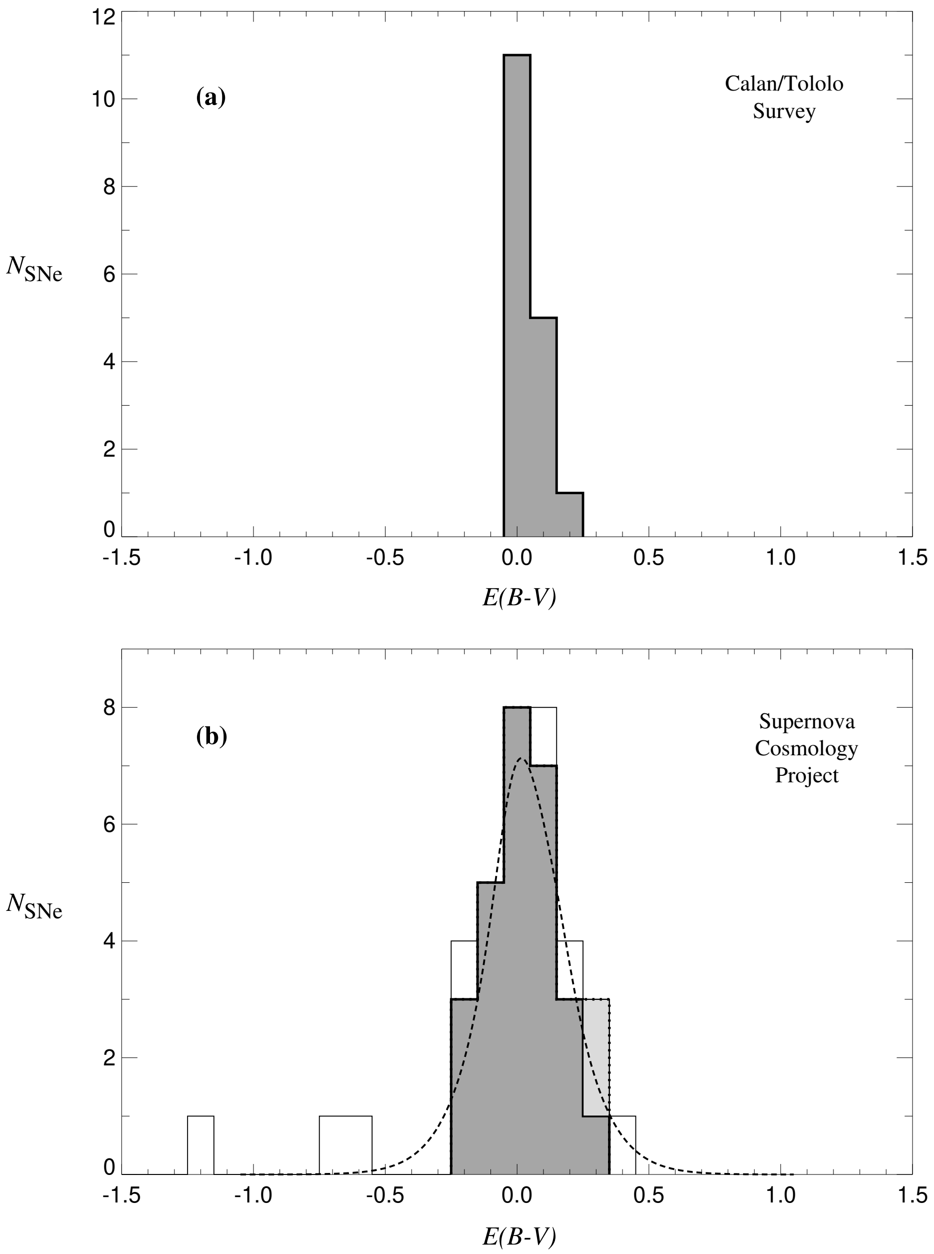

FIG. 6.— (a) The restframe $B-V$ color excess distribution for 17 of 18 Calán/Tololo supernovae (see text), corrected for Galactic extinction using values from Schlegel *et. al.* 1998. (b) The restframe $B-V$ color excess for the 36 high-redshift supernovae for which restframe $B-V$ colors were measured, also corrected for Galactic extinction. The darker shading indicates those $E(B-V)$ measurements with uncertainties less than 0.3 mag, unshaded boxes indicate uncertainties greater than 0.3 mag, and the light shading indicates the two supernovae that are likely to be reddened based on their joint probability in color excess and magnitude residual from Fit B. The dashed curve shows the expected high-redshift $E(B-V)$ distribution if the low-redshift distribution had the measurement uncertainties of the high-redshift supernovae indicated by the dark shading. Note that most of the color-excess dispersion for the high-redshift supernovae is due to the rest-frame V-band measurement uncertainties, since the rest-frame B-band uncertainties are usually smaller.

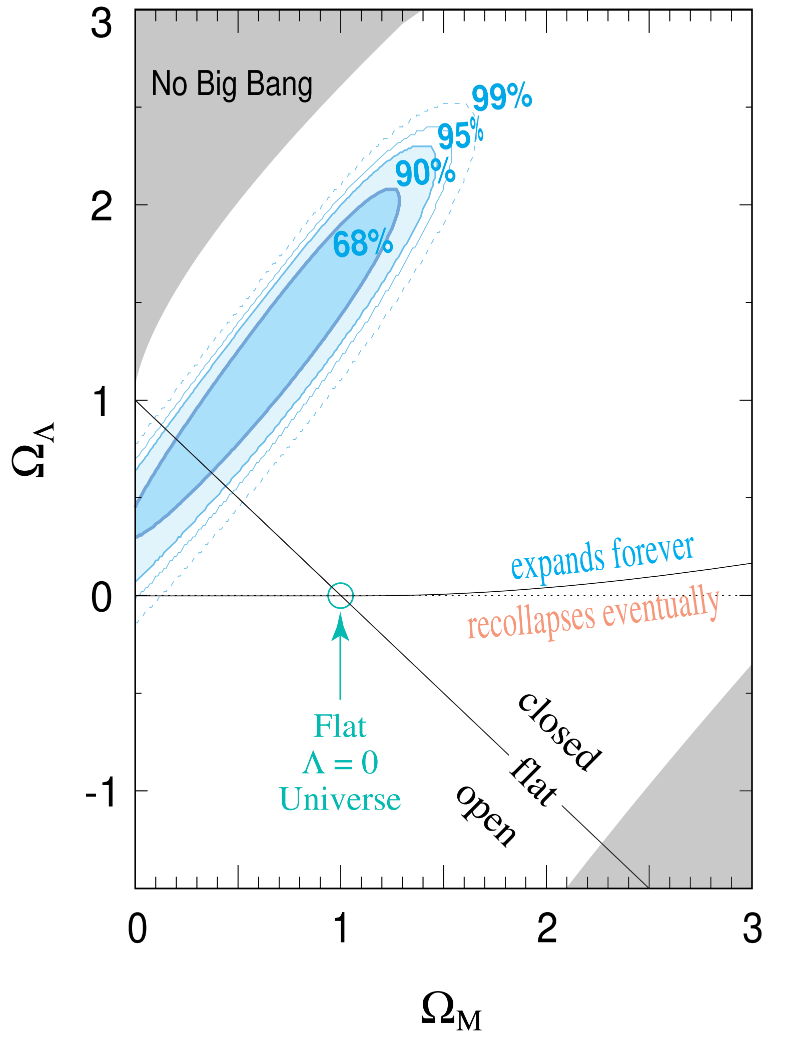

FIG. 7.— Best-fit confidence regions in the Ω_M–Ω_Λ plane for our primary analysis, Fit C. The 68%, 90%, 95%, and 99% statistical confidence regions in the Ω_M–Ω_Λ plane are shown, after integrating the four-dimensional fit over $\mathcal{M}_B$ and α. (The table of this two-dimensional probability distribution is available at http://www-supernova.lbl.gov/.) See Figure 5(e) for limits on the small shifts in these contours due to identified systematic uncertainties. Note that the spatial curvature of the universe—open, flat, or closed—is not determinative of the future of the universe's expansion, indicated by the near-horizontal solid line. In cosmologies above this near-horizontal line the universe will expand forever, while below this line the expansion of the universe will eventually come to a halt and recollapse. This line is not quite horizontal because at very high mass density there is a region where the mass density can bring the expansion to a halt before the scale of the universe is big enough that the mass density is dilute with respect to the cosmological constant energy density. The upper-left shaded region, labeled "no big bang," represents "bouncing universe" cosmologies with no big bang in the past (see Carroll, Press, & Turner 1992). The lower right shaded region corresponds to a universe that is younger than the oldest heavy elements (Schramm 1990), for any value of $H_0 \geq 50$ km s^{-1} Mpc^{-1}.

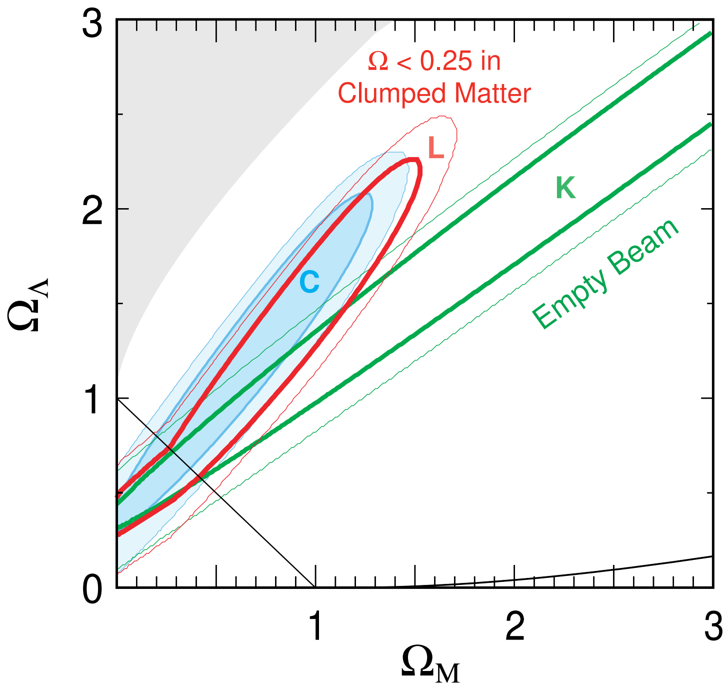

FIG. 8.— Best-fit 68% and 90% confidence regions in the Ω_M–Ω_Λ plane for cosmological models with small scale clumping of matter (e.g., in the form of MACHOs) compared with the Friedman-Robertson-Walker model of Fit C, with smooth small-scale matter distribution. The shaded contours (Fit C) are the confidence regions fit to a Friedman-Robertson-Walker magnitude-redshift relation. The extended confidence strips (Fit K) are for a fit of the Fit C supernova set to an "empty beam" cosmology, using the "partially filled beam" magnitude-redshift relation with a filling factor $\eta = 0$, representing an extreme case in which all mass is in compact objects. The Fit L un-shaded contours represent a somewhat more realistic partially-filled-beam fit, with clumped matter ($\eta = 0$) only accounting for up to $\Omega_M = 0.25$ of the critical mass density, and any matter beyond that amount smoothly distributed (i.e., η rising to 0.75 at $\Omega_M = 1$).

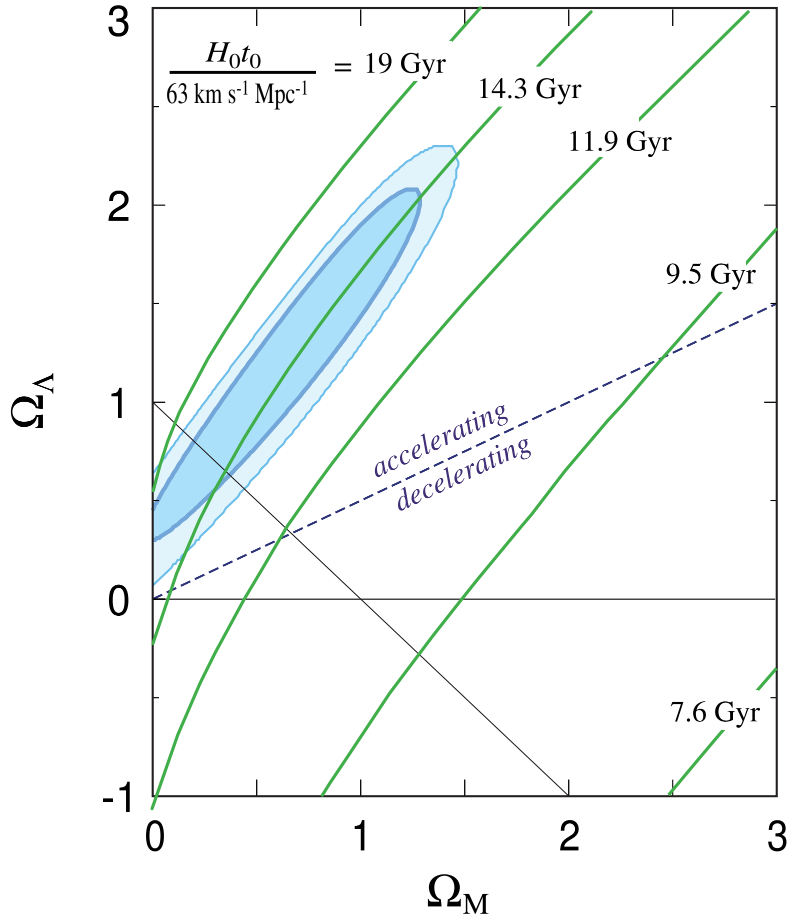

FIG. 9.— Isochrones of constant $H_0 t_0$, the age of the universe relative to the Hubble time, H_0^{-1}, with the best-fit 68% and 90% confidence regions in the Ω_M–Ω_Λ plane for the primary analysis, Fit C. The isochrones are labeled for the case of $H_0 = 63$ km s^{-1} Mpc^{-1}, representing a typical value found from studies of SNe Ia (Hamuy et al. 1996; Riess, Press, & Kirshner 1996; Saha et al. 1997; Tripp 1998). If H_0 were taken to be 10% larger (i.e., closer to the values in Freedman et al. 1998), the age labels would be 10% smaller. The diagonal line labeled accelerating/decelerating is drawn for $q_0 \equiv \Omega_M/2 - \Omega_\Lambda = 0$, and divides the cosmological models with an accelerating or decelerating expansion at the present time.

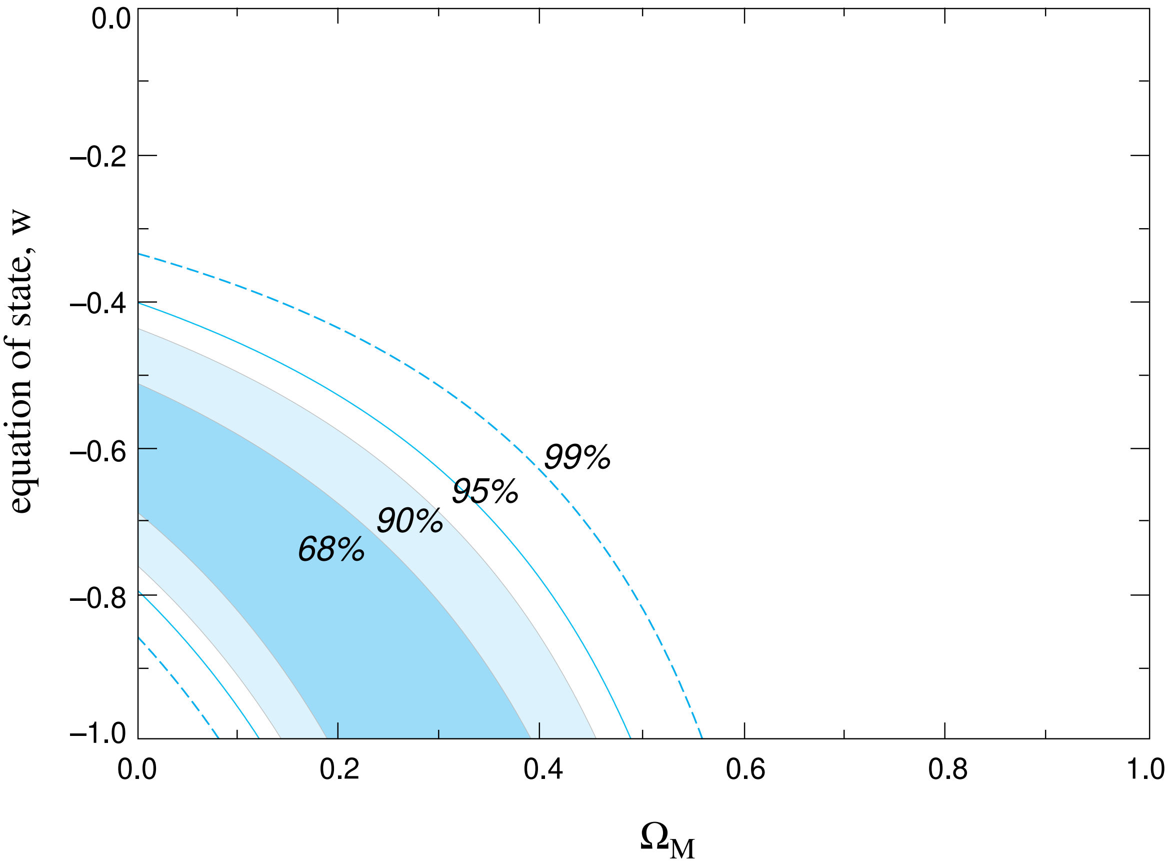

FIG. 10.— Best-fit 68%, 90%, 95%, and 99% confidence regions in the Ω_M–w plane for an additional energy density component, Ω_w, characterized by an equation-of-state $w = p/\rho$. (If this energy density component is Einstein's cosmological constant, Λ, then the equation of state is $w = p_\Lambda/\rho_\Lambda = -1$.) The fit is for the supernova subset of our primary analysis, Fit C, constrained to a flat cosmology ($\Omega_M + \Omega_w = 1$). The two variables $\mathcal{M}_B$ and α are included in the fit, and then integrated over to obtain the two-dimensional probability distribution shown.